LOW TEMPERATURE THERMAL CONDUCTIVITY OF IRRADIATED AND SWEPT SYNTHETIC QUARTZ

By

MOHAMMAD-REZA JALILIAN-NOSRATY

Bachelor of Science
University of Mashhad
Mashhad, Iran
May, 1972

Master of Science
Oklahoma State University
Stillwater, Oklahoma
July, 1977

Submitted to the Faculty of the Graduate College
of the Oklahoma State University
in partial fulfillment of the requirements
for the Degree of
DOCTOR OF PHILOSOPHY
May, 1980

TO

MY PARENTS

LOW TEMPERATURE THERMAL CONDUCTIVITY OF IRRADIATED

AND SWEPT SYNTHETIC QUARTZ

Thesis Approved:

Joel J. Martin
Thesis Adviser

George S. Dieter

Zuhair al-Shaieb

Timothy M Wilson

Norman N. Durham
Dean of the Graduate College

PREFACE

This study was concerned with the measurement of the thermal conductivities of synthetic quartz. Thermal conductivity measurements were taken for an Electronic grade sample, EG-S, and a Premium Q, PQ-S, over the range of 4.5 to 140K. Premium Q sample, PQ-E11 was run over the 1.6 to 48K range of temperature. A helium pot system and a variable heat leak system were used to cover this temperature range. The effects of radiation damage at room temperature and of electrolyzing in the presence of hydrogen were studied.

The author wishes to express his appreciation to his major adviser, and Committee Chairman, Professor J. J. Martin, for his guidance and assistance throughout this study. Appreciation is also expressed to the other committee members, Professor G. S. Dixon, Professor T. M. Wilson and Professor Z. Al-Shaieb, for their guidance.

Finally, special thanks are expressed to my wife, Pooran, who made my life easy to complete this study and special thanks are expressed to my parents for their support and encouragement.

TABLE OF CONTENTS

LIST OF TABLES

LIST OF FIGURES

CHAPTER I

INTRODUCTION

α-Quartz

α-Quartz has trigonal symmetry and belongs to the enantiomorphous crystal class 32. Quartz occurs in both right handed and left handed forms, which are the mirror image of each other (1,2). Figure 1 shows structure of right hand quartz. α-Quartz is a piezoelectric material and is widely used as a frequency control device. Synthetic α-quartz crystals are hydrothermally grown (3).

All quartz contains aluminum as a substitutional (for silicon) impurity. The aluminum requires charge compensation. In as-grown material interstitial alkali ions are the dominant charge compensation. Hydrogen in the form of OH is also present in as-grown material but it does not seem to be at the aluminum site. Irradiation at temperatures above 200K will replace the alkali with a proton on the neighboring oxygen forming the Al-OH centers (4). The aluminum-hole center $[Al_{e+}]^{o}$, is also formed by irradiation in this same temperature region (5). Annealing this irradiated as-received sample at 450°C for a few minutes restores it to its original condition. If the as-grown material is irradiated at temperatures below 200K the Al-Na defect is stable and only a few $[Al_{e+}]^{o}$ center are produced.

At high temperatures ($T \geq 400^{o}C$) the interstitial alkalis which are in the large Z (or C) axis channels become mobile. If an electric field

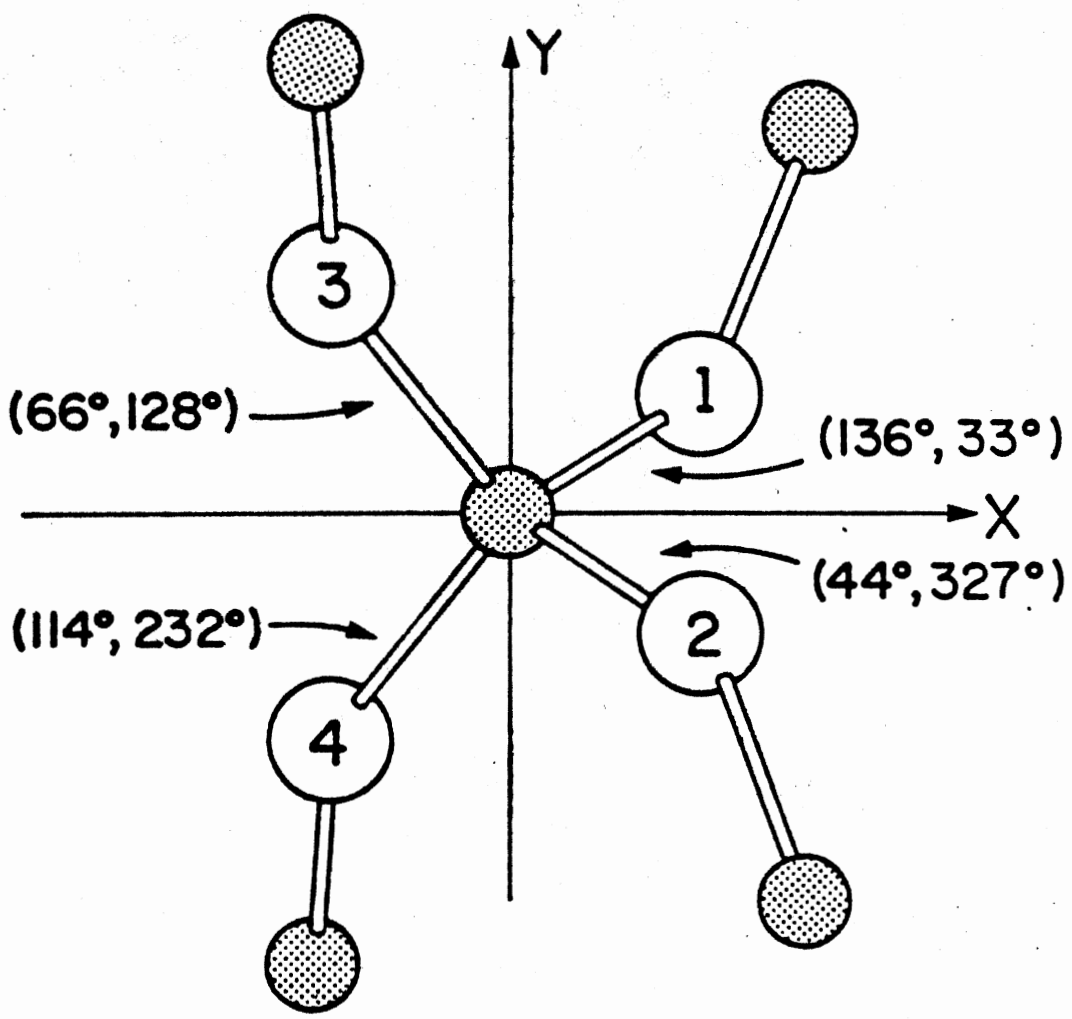

(θ with respect to Z axis, ϕ with respect to X axis)

Figure 1. Structure of Distorted Si-O Tetrahedron

is applied along the Z axis the alkalis can be swept out of the crystal and are replaced by protons. These protons form an OH^- molecule by being on the non-bonding P orbital of a nearest neighbor (to the aluminum) oxygen atom. This electrolyses or sweeping process was first used by King (6) to "purify" natural quartz. The process has also been used by Kats (7) and by Fraser (8) to sweep specific alkali ions into the crystal. Recent work by Capone et al. (9) has shown that electrolyzed quartz oscillator crystals show increased radiation hardness. Irradiation of conventionally swept quartz at temperatures below 200K produces large amounts of $[Al_{e+}]^o$ centers as the proton is easily removed from the aluminum site (5). Irradiation at room temperature produces some $[Al_{e+}]^o$ centers but the Al-OH centers are also present. The relative concentration of Al-OH and $[Al_{e+}]^o$ centers after a room temperature irradiation will depend upon the depth of the available electron traps.

Berman (10) has reported the earliest low temperature thermal conductivity studies of natural quartz and of the effects of radiation damage on the thermal conductivity. He found that the effect of impurities in good natural quartz is small and that the thermal resistance above 10K is mainly due to Umklapp processes. He also found that the damage produced by neutron bombardment strongly suppressed the thermal conductivity maximum. He observed that the thermal conductivity maximum was partially restored by a thermal anneal. Fraser (11) has reported some more recent unpublished results obtained by Berman on some synthetic quartz samples. These synthetic samples showed very low thermal conductivities with maximum values around 1.5 W/cm K. Zeller and Pohl (12) in their work on the thermal conductivity and specific heat of glasses have measured the thermal conductivity of a high quality natural

quartz sample with the heat flow parallel to the Z axis. They found a maximum thermal conductivity near 30 W/cm K and that the thermal conductivity went as T^3 over the 0.1K to 5K temperature range.

Recently Wasim and Nava (13) have investigated the effect of γ-irradiation on the low temperature thermal conductivity of natural quartz. Their as-received sample showed thermal conductivities in good agreement with the results of Zeller and Pohl. After room temperature γ-irradiation at doses up to 10^8 rad. they observed a strong dip in the thermal conductivity curve growing in between 5 and 7K. They interpreted this dip as being caused by phonon scattering due to extended defects produced by the irradiation.

Present Study

The thermal conductivity of premium Q synthetic quartz will be measured over the range 1.5K to 50K temperature range. Also measurements will be done for less pure samples (as-received and irradiated) over the 1.5K to 120K temperature range. The heat flow will be along the Y axis. The thermal conductivities of Sawyer Premium Q quartz and Sawyer Electronic grade quartz will be compared. The effects of irradiation of these samples will also be investigated. Wasim and Nava (13) have found that γ-irradiation of natural quartz at room temperature causes a dip in the thermal conductivity curve between 5 and 7K. They have interpreted their results in terms of phonon scattering by extended defects. A series of investigations (4,5,14,15) by the Oklahoma State University quartz project has shown that a room temperature irradiation of synthetic quartz produces both Al-OH center and $[Al_{e^+}]^\circ$ centers. Both of these centers might produce resonant phonon scattering. A well characterized

Premium Q sample will be irradiated at room temperature and its thermal conductivity measured from 1.5K to 45K in order to compare with the work of Wasim and Nava (13). After the irradiation experiment this sample will be electrolyzed in hydrogen. This process will remove all alkalis (and, also, holes) and the dominant defect will then be the Al-OH center. After sweeping the sample will be run over the 1.5K to 13K temperature range. By these tests it should be possible to determine whether or not the dip in the thermal conductivity curve is caused by Al-OH centers. The results for the sample after sweeping will also be compared with the results in the as-received condition and with electronic grade sample.

CHAPTER II

THEORY OF LATTICE THERMAL CONDUCTIVITY

Introduction

There are several mechanisms by which heat can be transmitted through a solid and many processes which limit the effectiveness of each mechanism. In a non-metal heat is conducted by means of the thermal vibration of the atoms (elastic waves) often called phonons. If the phonon distribution is not in equilibrium throughout the solid, a net flow of heat results giving rise to thermal conduction. In a simple metal this mode of heat transport makes some contribution, but the observed thermal conductivity is almost entirely due to the electrons.

The thermal conductivity of materials in which the heat is carried by phonons, has been qualitatively understood for many years. In a crystal lattice it should be theoretically possible to determine exact values for the thermal conductivity, λ, if the entire phonon spectrum and the anharmonicity of the lattice forces of the crystal were completely known in detail. However, very little is known about the lattice force anharmonicity, so it is nearly impossible to do a first principles theoretical calculation of the lattice thermal conductivity. Fortunately, several phenomenological models have been developed which greatly add to the understanding of the basic processes. These models

can be readily used to interpret experimental results. Reviews of the theory of thermal conductivity in solids have been given by Klemens (16,17), Carruthers (18), and Ziman (19).

Kinetic Theory Approach

In 1914 Debye (20) regarded the heat as transmitted by waves formed the lattice vibrations. The appropriate mean free path is the distance such a wave travels before its intensity is attenuated by scattering to $\frac{1}{e}$ of its initial value. If a "phonon gas", is assumed an expression for the thermal conductivity, λ, can be obtained by analogy to the kinetic theory of gases,

$$\lambda = \frac{1}{3} cv\ell \tag{1}$$

or, with $\ell = v\tau$,

$$\lambda = \frac{1}{3} cv^2\tau \tag{2}$$

where v is the velocity of sound in the material, c is the specific heat of the material, ℓ is the phonon mean-free path, and τ is the phonon relaxation time between the various scattering processes. One assumption made in transfering this kinetic theory model to phonons is that there is no dispersion.

At high temperatures ℓ is limited by direct interaction among the phonons themselves, and at sufficiently high temperatures ℓ is inversely proportional to T. As the temperature decreases, the interactions among the phonons become less effective in restricting ℓ, which thus increases more rapidly than $\frac{1}{T}$. For sufficiently perfect crystals this increase is best represented by an exponential of the form

$\ell \alpha \exp(T^*/T)$, where T^* is a characteristic temperature for the particular crystal and is an appreciable fraction of the Debye characteristic temperature. At easily accessible low temperatures (~1 to ~10K, depending upon the material) ℓ may reach several millimeters and is thus comparable with the smallest dimensions of most specimens studied. It then tends to a constant value which depends on the shape and size of the specimen.

In order to deduce the behavior of the thermal conductivity from that of the mean free path, we must introduce the temperature variation of the heat capacity. The mean velocity can often be regarded as independent of the temperature. At temperatures which are high enough for the relation $\ell \alpha \frac{1}{T}$ to hold, c is nearly constant so that $\lambda \alpha \frac{1}{T}$. As the temperature decreases, c also decreases eventually becoming proportional to T^3. If the temperature is not too low the exponential variation in ℓ will dominate so that the conductivity nearly exponential in T^{-1}. Finally, when the mean free path becomes constant the temperature dependence of the conductivity reflects the T^3 behavior of the specific heat.

In 1929, Peierls (2), in the first quantum mechanical treatment of lattice conduction introduced the concept of phonons (quantized lattice vibrations). He also pointed out the role of Umklapp phonon-phonon scattering in limiting the thermal conductivity. If the kinetic theory expression, Eq. 2, is generalized or if the Boltzmann transport equation (16,19,23-25) is solved in the relaxation time approximation the thermal conductivity, λ, can be expressed as a sum over all lattice modes

$$\lambda = \frac{1}{3} \sum_{i,q} c_i(q)\, v_{q,i}^2\, \tau_{q,i} \quad . \tag{3}$$

In Eq. (3) $c_i(q)$ is the specific heat per unit volume for a phonon of wave vector q and polarization i, $v_{q,i}$ is phonon group velocity and $\tau_{q,i}$ is the corresponding relaxation time. If polarization is ignored Eq. (3) can be written in terms of the phonons angular frequency, ω

$$\lambda = \frac{1}{3} \sum c(\omega)\, v_\omega^2\, \tau(\omega) \quad . \tag{4}$$

Klemens (16,17) applied the Debye approximation to Eq. (4). In the Debye approximation the three discrete acoustic phonon branches are replaced by a single continuous non-dispersive branch. This branch has the average sound velocity and a limiting frequency ω_D. Eq. (4) can then be written as

$$\lambda = \frac{1}{2\pi^2 v} \int_0^{\omega_D} \tau \frac{\hbar^2 \omega^4}{k\, T^2} \frac{e^{\hbar\omega/kT}}{\left(e^{\hbar\omega/kT} - 1\right)^2} d\omega \tag{5}$$

where k is Boltzmann's constant, $\hbar$ is Plank's constant over 2π and v is the average sound velocity.

Early comparisons between theory and experiment were performed by using Eq. (5) and the relaxation time, $\tau(\omega,T)$ for a particular scattering process to calculate a thermal resistivity for that process (22,23). The total thermal resistivity was found by adding the thermal resistivities for the various scattering processes. If the scattering processes are independent the reciprocals add (scattering probabilities) and a combined relaxation time can be found.

$$\tau^{-1} = \sum_i \tau_i^{-1}(\omega,T) \tag{6}$$

where $\tau_i(\omega,T)$ is the relaxation time for the $i^{\underline{th}}$ process. The digital computer has made it possible to numerically evaluate Eq. (5) with the combined relaxation time given in Eq. (6). This numerical technique was first used by Callaway (25).

Scattering Processes

Boundary Scattering

According to the theory of Peierls (21) for phonon-phonon interaction as the temperature decreases the thermal resistance of insulating crystal must decrease rapidly. However, this result will hold only for an infinite lattice. According to his theory for a given crystal of finite dimensions there will always be a temperature below which the mean free path of the elastic waves becomes comparable to the dimensions of the crystal. When this happens the elastic waves will be scattered by the boundaries of the crystal and the thermal conductivity will be finite.

The first experimental data which supported this theory was found by de Haas and Biermasz (26). Casimir (27) derived the relaxation time for boundary scattering from diffuse surfaces.

$$\tau_B^{-1} = \frac{V}{L} \tag{7}$$

where V is the average sound velocity and L is an effective diameter which depends upon the sample geometry. In the Debye-Callaway approach the average sound velocity is given by

$$\frac{1}{v} = \frac{1}{3}\left(\frac{2}{v_t} + \frac{1}{v_\ell}\right) \tag{8}$$

where v_t and v_ℓ are respectively the transverse and longitudinal sound velocities. For a "perfectly rough" rectangular sample

$$L = 2\pi^{-\frac{1}{2}}(a \cdot b)^{\frac{1}{2}} \tag{9}$$

where a and b are the dimensions of the sample's cross section perpendicular to the heat flow. Equation (9) is based upon the assumption that the crystal is long compared to a and b. For the samples which are not "perfectly rough", an increase in the measured thermal conductivity will be observed because specular reflections of the phonons will occur (28). If the sample's length is of the order of its other dimensions, then a correction for reflection off the crystal's ends must be made (28). When all the phonons mean-free-path are comparable to the sample's cross-sectional dimensions (at low enough temperatures), the relaxation time is usually entirely limited by the boundary scattering, which is temperature and frequency independent. For this range of temperature the thermal conductivity will vary as T^3 (27,29). Other scattering mechanisms such as clusters (30), bubbles (31), grain boundaries (32), colloids (33-35), mosaic substructures (36) and possibly certain types of magnetic impurity scattering (37-39) can also cause a T^3 temperature dependence.

Point Defects

A defect which extends over a volume with linear dimensions much smaller than the phonon wavelength can be considered as a point defect. A defect which fits this criterion may be a vacant lattice site, an interstitial atom, an impurity atom, or an isotope of the specimen whose atomic weight is different from that of the majority of atoms,

or combination of these. These point defects will upset the regularity of the crystal lattice and at low temperatures this irregularity which will be much smaller than the phonon wavelength will produce the scattering which is analogous to the effect in optics known as Rayleigh scattering (40). For point defects Klemens found

$$\tau_{PD}^{-1} = A\,\omega^4 \tag{10}$$

where ω is the phonon frequency. Klemens determined an expression for A for mass defect scattering due to isotopes in elements. Slack (41) has modified Klemens expressions for A for elemental materials to include compounds. For a compound $A_x B_y C_z \ldots\ldots$

$$A = \frac{\delta\Gamma}{4\pi v^3} \tag{11}$$

where v is the velocity of sound in the material and δ is the cube root of the atomic volume and Γ is

$$\Gamma = \Sigma \frac{x}{x+y+z\ldots.} \left(\frac{M_A}{\bar{M}}\right)^2 \Gamma_A + \frac{y}{x+y+\ldots.} \left(\frac{M_B}{\bar{M}}\right)^2 \Gamma_B + \cdots\cdots \tag{12}$$

where

$$\Gamma_A = \sum_i f_i \left(\frac{\Delta M_i}{\bar{M}_A}\right)^2 ; \tag{13}$$

M_A and M_B are the masses of the isotopes of the atoms of types A and B respectively, $\bar{M}_A$ and $\bar{M}_B$ are the average masses of these atoms, and M is the average molecular mass defined as

$$\bar{M} = \frac{XM_A + yM_B + \cdots}{x+y+\cdots} \tag{14}$$

f_i is the isotopic aboundance of the ith isotope, and ΔM_i is the difference between the mass of the ith isotope and the average mass. Point defect scattering affects the peak of the thermal conductivity curve. Usually the Rayleigh scattering relaxation time will give us a qualitative estimate of the scattering strength.

Phonon-Phonon Interaction

In a perfectly harmonic crystal, the potential energy of an atom is exactly quadratic in the displacement from equilibrium. Consequently, there would be no interaction between thermal waves, and no tendency for an arbitrary phonon distribution to return to the equilibrium distribution. The result is an infinite thermal conductivity. However, experiment shows that the thermal conductivity is finite, and, therefore, the potential is not strictly quadratic in the atomic displacements. This anharmonic potential causes the three phonon interaction which limits the thermal conductivity. There are two types of these interactions, normal processes and Umklapp processes. In both phonon-phonon interaction energy is conserved.

The three phonon normal processes are the only phonon-phonon interaction which conserve momentum. Normal process can be described by the equation

$$\vec{q}_1 + \vec{q}_1 = \vec{q}_3 \tag{15}$$

where $\vec{q}_1$ and $\vec{q}_2$ are the wave vectors of the incoming phonons and $\vec{q}_3$ is the wave vector of the outgoing phonon. Since normal processes pre-

serve the direction of the energy transfer by the phonons involved, they do not directly limit the thermal conductivity (24). Callaway (25) has discussed the possibility that nromal processes will, however, aid other phonon interactions. Herring has derived the frequency and temperature dependence for a number of low wave vector normal process interactions (22).

Peierls (21) suggested the process

$$\vec{q}_1 + \vec{q}_2 = \vec{q}_3 + \vec{G} \tag{16}$$

where $\vec{G}$ is reciprocal lattice vector. This process known as umklapp (flip over) process changes the direction of energy transfer and, therefore, limits the thermal conductivity. Since $\vec{q}_1 + \vec{q}_2$ must extend outside the first Brillouin zone, at least one of them must have q greater than one half the wave vector of a zone boundary phonon. This argument led Klemens (16) to estimate that the processes rate was proportional to $\exp(-\frac{\theta}{\alpha T})$ in the Debye approximation, here α is an integer equal or greater than two and θ is the Debye temperature. This term occasionally in very pure materials gives rise to a thermal conductivity proportional to $\exp(\theta/T)$.

Many different forms have been suggested for the relaxation time forms, such as

$$\tau_u^{-1} = B_1 T^3 \omega^2 e^{-\theta/aT} \tag{17}$$

$$\tau_u^{-1} = B_1 T^2 \omega^2 e^{-\theta/aT} \tag{18}$$

these have been suggested by Callaway (25), and Berman and Braks (28) respectively. Parameter B_1 is a "fitted" parameter. Other forms also

have been suggested by Klemens (16), for high temperature he finds

$$\tau_u^{-1} = B_1 T\omega^2$$

At high temperatures where the umpklapp processes are dominant, the thermal conductivity curve usually follows as T^{-1} dependence. It is often found (43-45) that a phonon-phonon scattering, relaxation time, τ_{pp}^{-1}, of the form

$$\tau_{pp}^{-1} = (B_1 + B_2 e^{-\theta/aT})\omega^2 T \tag{19}$$

where B_1, B_2 and a are fitted parameters, can be used to fit the experimental results over a wide range of temperatures.

Resonance Scattering

Certain point defects can introduce local vibrational modes into the crystal. These modes can cause a resonant scattering of the phonons which carry the thermal current. The resonant scattering causes a dip in the thermal conductivity curve at a temperature where the average thermal phonon is in resonance with the local mode. Pohl (35,46,47) suggested (35,46,47) that the proper form of relaxation time for resonance scattering can be written as

$$\tau_r^{-1} = \frac{F\omega^2 T^P}{(\omega^2-\omega_o^2)^2 + (\frac{\Omega}{\pi})^2 \omega^2\omega_o^2} \tag{20}$$

F is resonance parameter, ω_o is the resonant frequency, Ω describes the damping, P = O has been used for dips at temperature below the thermal conductivity maximum and P = 2 for temperature above maximum. Pohl used

Eq. (20) to describe resonant scattering in a number of doped alkali halides. He found that the damping term could usually be ignored.

Summary

In the present work, the following scattering processes were included in the calculation of the thermal conductivity of quartz boundary scattering, isotope scattering, phonon-phonon scattering and finally resonance scattering. The total relaxation time which was used in Eq. (5) was

$$\tau^{-1} = \frac{v}{L} + A\,\omega^4 + (B_1 + B_2\, e^{-\theta/aT})\,\omega^2 T + \frac{F\omega^2}{(\omega^2 + \omega_o^2)^2} \qquad (21)$$

CHAPTER III

EXPERIMENTAL PROCEDURE

Apparatus

In order to measure the thermal conductivity of quartz over a large temperature range two separate systems were used. Both systems employed the standard longitudinal steady-state heat flow technique (48). In the simplest steady-state experimental arrangement, shown in Figure 2, heat is supplied at one end of a rod of uniform cross-sectional area A at a known rate $\dot{Q}$ and is removed at the other end. Thermometers are attached at two places along the specimen separated by a distance Δx, and the temperature difference ΔT between them is measured. The conductivity is then derived from the relation

$$\dot{Q} = \lambda \frac{A\Delta T}{\Delta x} \tag{22}$$

where λ is thermal conductivity. A variable heat leak system was used to cover the 3.5 K to 140 K temperature range, and a helium pot system was used for 1.5K to 4K.

Variable Heat Leak System

The apparatus consists of a glass cryostat and a sample holder. A diffusion pump and mechanical roughing pump vacuum system was used to evacuate the cryostat and sample holder. A separate mechanical pump was

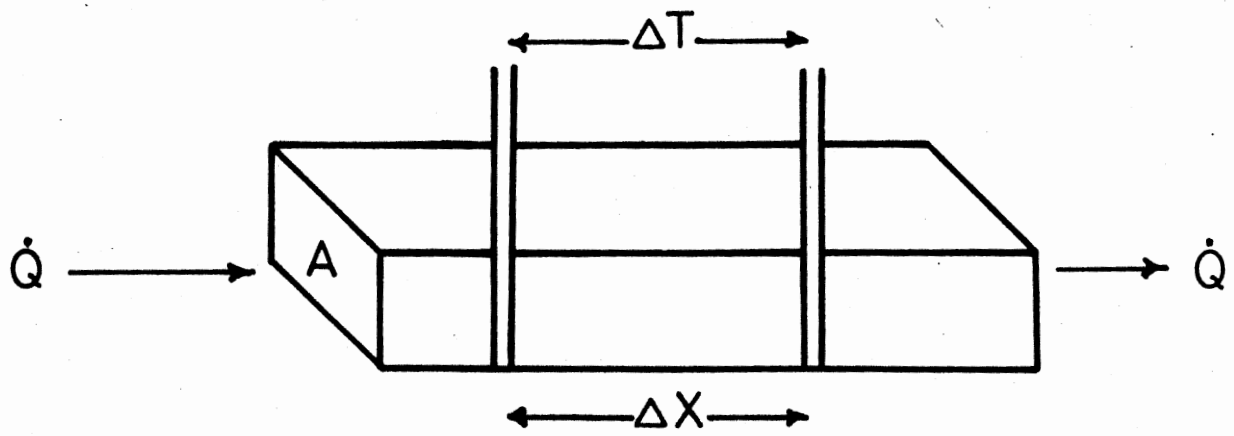

Figure 2. Principle of the Steady-State Longitudinal Heat-Flow Method for Measuring Thermal Conductivity

used to pump on the cryogenic bath. By using this pump the 3.5K to 5K region could be covered with liquid helium as well as the 50K to 77K region with liquid nitrogen.

A schematic diagram of the cryostat and sample holder is shown in Figure 3. The cryostat contains four chambers. They are as follows: 1 - Exterior vacuum chamber to isolate the liquid nitrogen chamber from the room temperature. 2 - A chamber with a cylindrical hole in its top to put in liquid nitrogen. 3 - Interior vacuum chamber to isolate the inner chamber from the last nitrogen one. 4 - The helium chamber. The sample holder is placed in the helium chamber. Depending upon the desired range of temperature (3.5 - 50K or 50 - 140K) we put either liquid helium or liquid nitrogen into the helium chamber. To cool the system prior transferring liquid helium, helium exchange gas is introduced into the vacuum space between the nitrogen and helium chambers.

Figure 4 shows the details of the sample holder. The sample holder consists of a small brass vacuum can which contains a heat sink, an ambient heater and the holder clamp for the sample. This can is sealed by Wood's metal on top, and from this top it has two stainless steel tubes which support the holder in the cryostat. One of these tubes carries cables to the meters and power supplies, and it is also used to evacuate the holder. The other one is used to pump out the variable heat leak. This heat leak is used to increase the temperature range over which measurements can be made with a given cryogenic liquid; it will be discussed in more detail later. There is a clamp at the bottom of this tube to hold the sample. There is an aluminum flange over the clamp on which is fixed a cylindrical aluminum heat shield to reduce thermal radiation. The electric ambient heater is wound on the tube

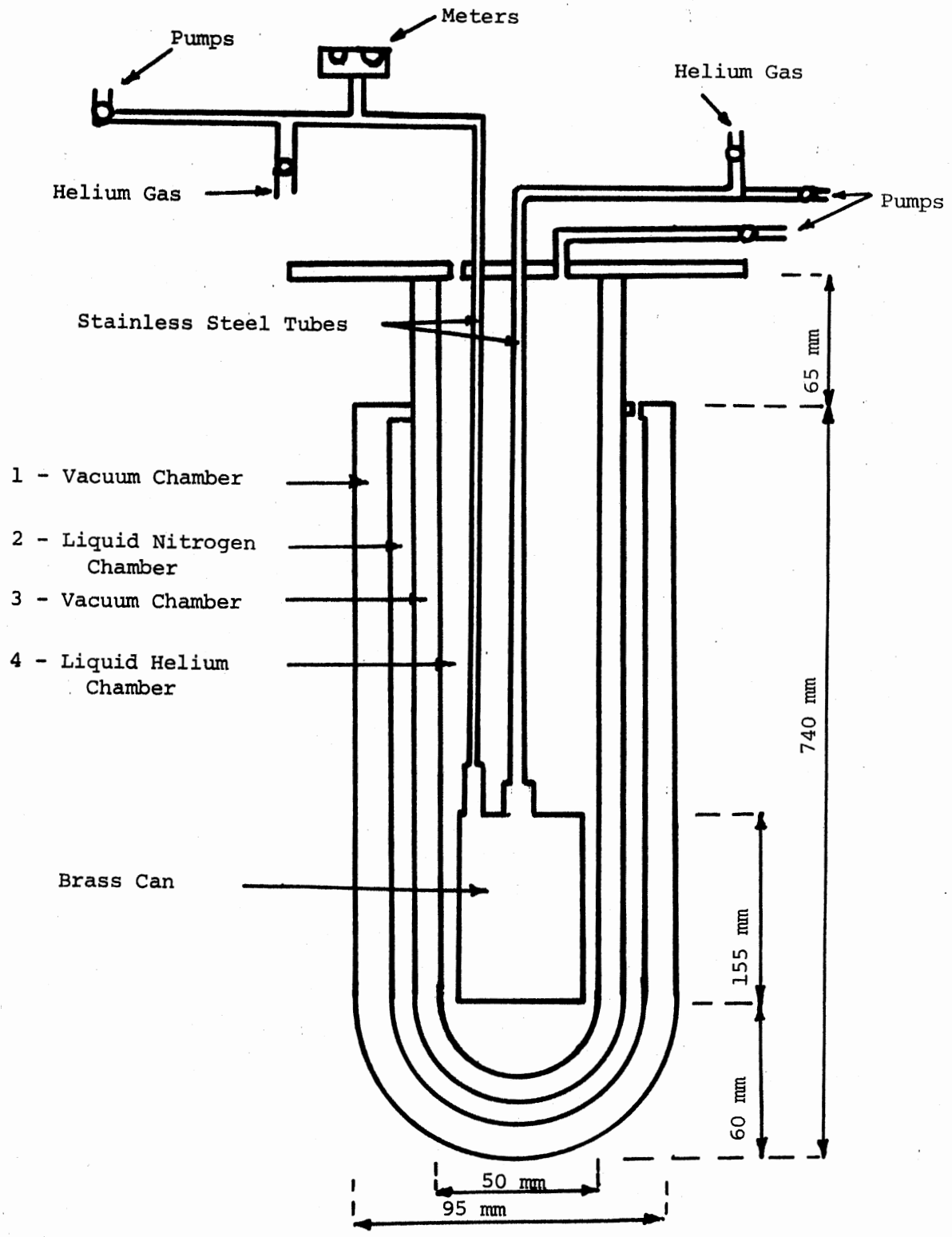

Figure 3. Cryostat and Sample Holder

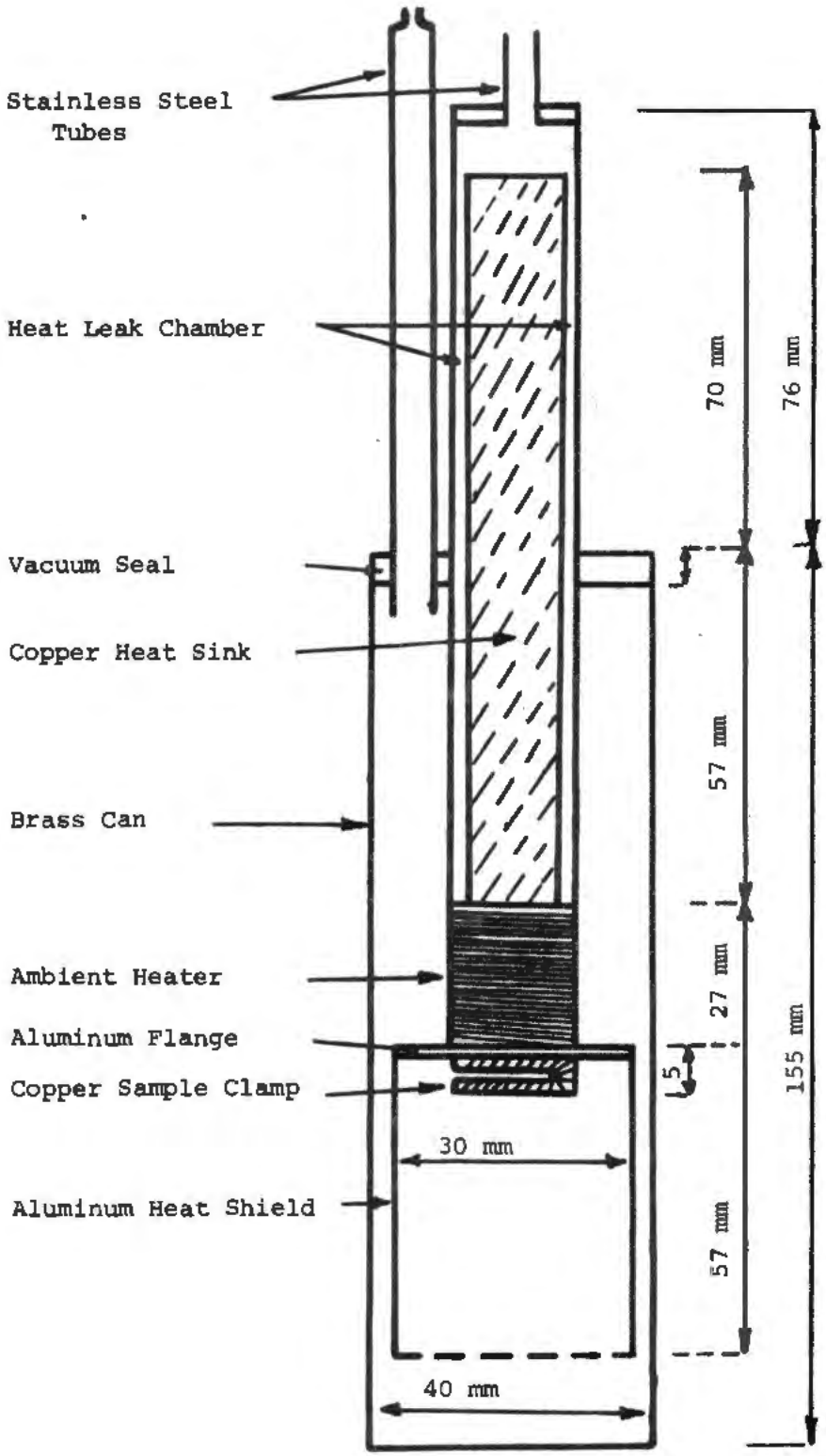

Figure 4. Thermal Conductivity Sample Holder for 3.5K to 140K

directly above the aluminum flange. Above this heater the tube has an internal copper cylindrical heat sink. A heat leak chamber is formed by the space between heat sink and the wall of the tube. Depending upon the temperature range the chamber may be filled with helium gas (for lower temperatures) or may be evacuated (for higher temperatures). If transfer gas is placed in the heat leak chamber the copper heat sink will be thermally anchored to the cryogenic bath which surrounds the holder. Thus, there will be a good thermal contact with the cryogenic bath and the copper rod will have nearly the same temperature as the bath. When the sample is heated by the ambient heater, the heat is quickly transferred into the bath, holding the sample near the bath temperature. Pumping some or all of the helium gas out of the heat leak chamber will reduce thermal contact between the copper heat sink and the cryogenic bath, then the heat transferred to the copper heat sink is not efficiently removed and the temperature of the heat sink and sample will rise. With a good vacuum in the heat leak chamber, the heat sink is effectively isolated from the cryogenic bath; therefore, temperatures much higher than the bath's can be reached. For example, measurements near 45K can be made with a liquid helium bath.

Figure 5 shows the detail of the sample and holder. For better thermal conductivity the sample is held in thermal contact with the heat sink by a copper clamp containing indium pads which were flattened against the sample when the nylon screws were tightened. A phosphor bronze spring and the nylon screws compensated for the difference in the thermal expansion between the sample and the clamp. The two thermometers are attached to clamps which are constructed in a similar manner. These thermometers are chromel versus gold-0.07 atomic percent

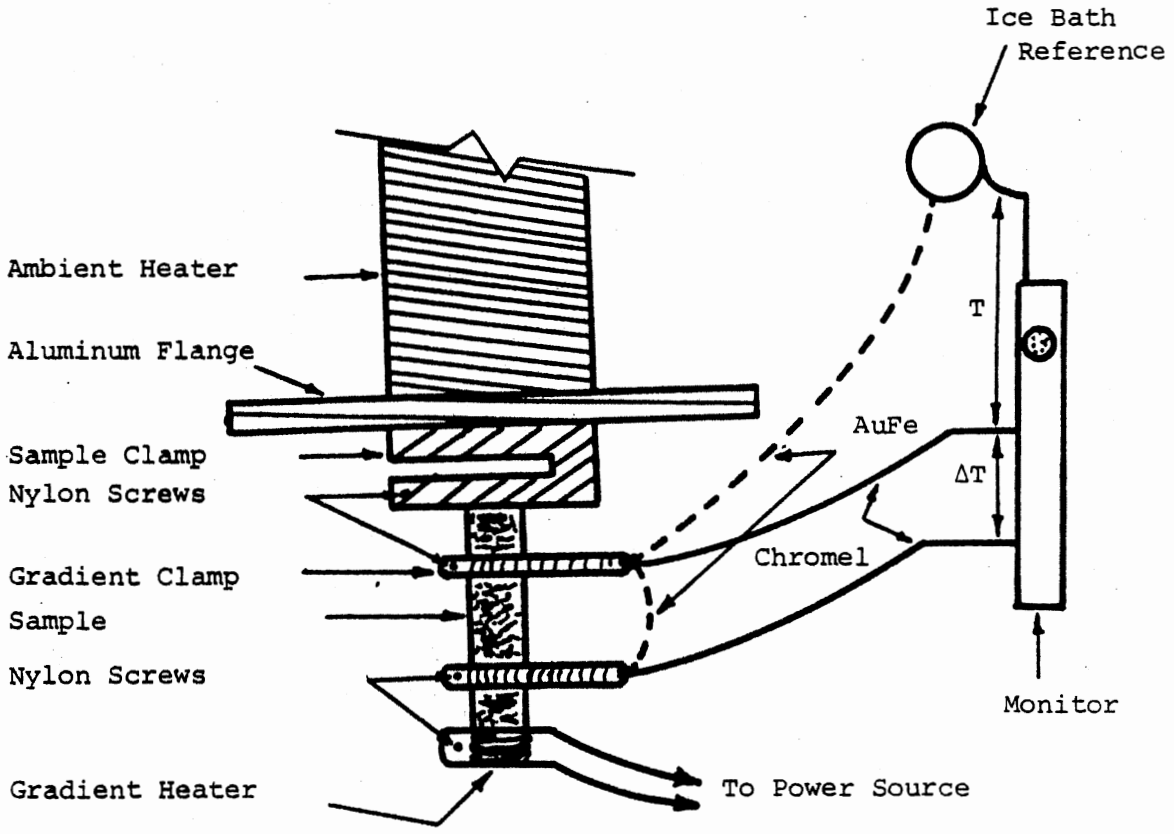

Figure 5. Detail of the Sample Holder With the Sample

iron. Indium is used to solder thermocouples to the clamps, which are shown in Figure 6. The emf's of the T and ΔT thermocouples are read directly by using potentiometers. A chromel versus gold-0.07 atomic percent iron versus chromel differential thermocouple was used to measure ΔT directly. The advantage of this connection is that the emf's measured do not depend on the difference of temperature between the sample and the ice bath reference. A detail of this connection is shown in Figure 5. The ambient temperature emf was measured with a Leeds and Northrup Type K-3 Universal Potentiometer and with a Leeds and Northrup 9834 D.C. Null Detector. This system has a resolution of 0.5 microvolt. The gradient temperature emf was measured with a Model 2770 Honeywell potentiometer, which also was in parallel with Leeds and Northrup Type K-3, and a Leeds and Northrup 9838 guarded nanovolt detector. This system has a resolution of 0.01 microvolt.

The gradient heater is fixed to the bottom of the sample. This thermal energy will flow through the sample in the form of heat to produce ΔT. The ambient heater in other hand will raise the temperature of sample, T, and maintain this temperature. The gradient heater voltage and current are monitored on a 4 digit D.C. millivolt digital panel meter.

Helium Pot System

In this sample holder the heat leak chamber is replaced by a 80 cm^3 volume pot in which liquid helium can be placed. Since the thermocouples are not sensitive enough at temperatures lower than $4^{o}K$ (49,50), Allen Bradley carbon resistors are used as thermometers. The same cryostat and pumping system is used. A mechanical pump is used to lower the

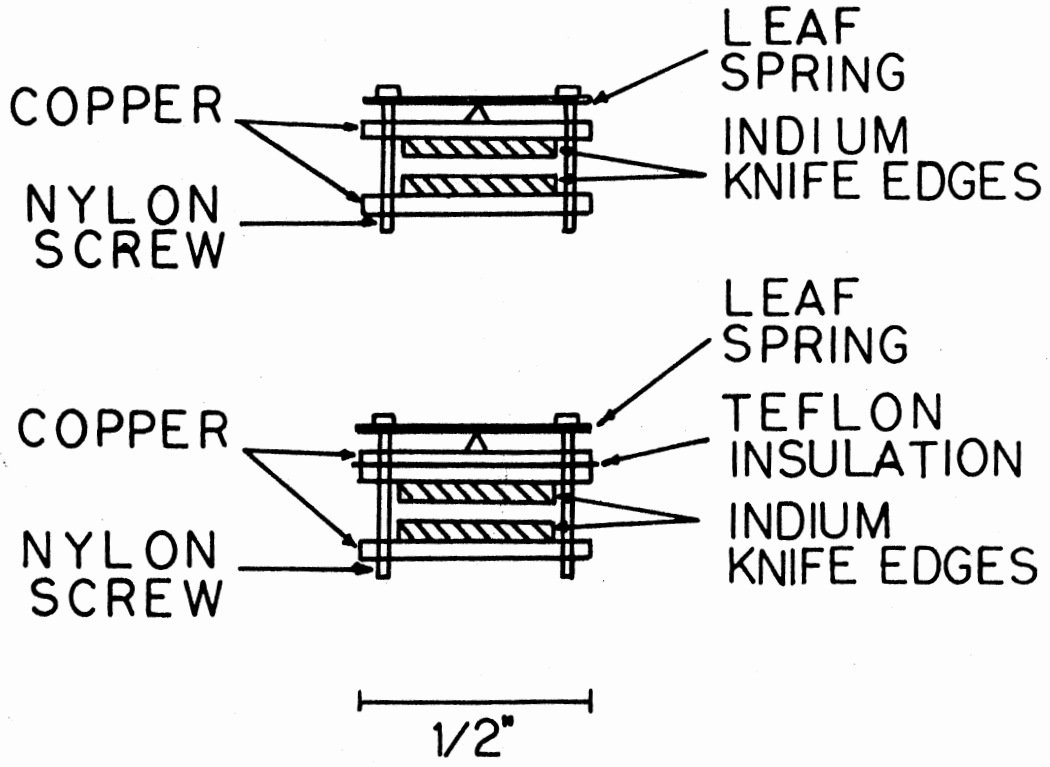

Figure 6. Detail of Sample, Thermocouple, and Carbon Resistance Thermometers Clamps

vapor pressure in the helium pot and, since the volume is small, the temperature can be easily reduced down to 1.5K. The temperature of the pot was monitored by using mercury and, at low pressures, oil U-tube monometers.

Figure 7 shows schematic of this sample holder. A small hole drilled through the vacuum seal leading into the stainless steel tube and a threaded brass rod with a point which could be screwed into this hole acted as a valve between the helium pot and the cryogenic bath. When the pointed brass rod was screwed into the hole the pot was effectively isolated from the bath. By adjusting the pumping speed of the pump we can get various temperatures between 1.5K to 4K. Since the vacuum in the sample chamber is better than 10^{-5} Torr the only thermal contact with the main liquid helium bath is through a thin-walled stainless tube, 2.5 cm long and the electrical leads.

As mentioned before in this apparatus instead of thermocouple thermometers, Allen Bradley carbon resistors are used. The same sample clamps were used for carbon resistors as before. The sample was installed in the sample holder in the same manner as before. The gradient heater was used. The ambient heater is wound around the helium pot and used only for small adjustments temperature.

Measurement of T and ΔT will be discussed later, in the measurements section. Briefly, we see that to get T and ΔT, we need to measure R and ΔR, the later will be produced by the gradient heater. To measure R and ΔR a resistance bridge circuit as shown in Figure 8 was set up. The coaxial wires are used to connect the sample holder to these circuits and to the lock-in amplifier which was used as the bridge null-detector. Coaxial cables were needed to prevent ac pick-up.

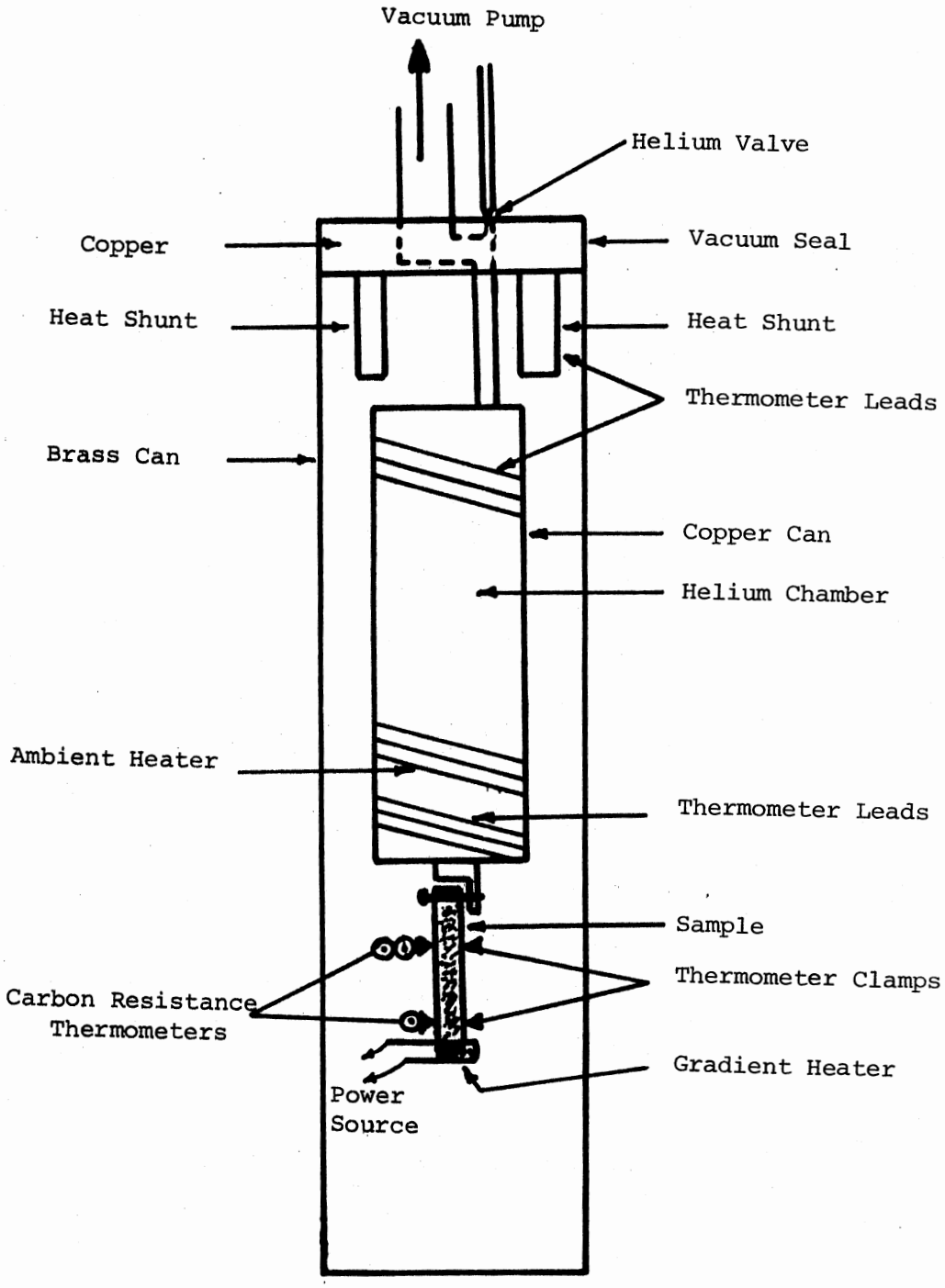

Figure 7. Thermal Conductivity Sample Holder for 1.5 to 4K

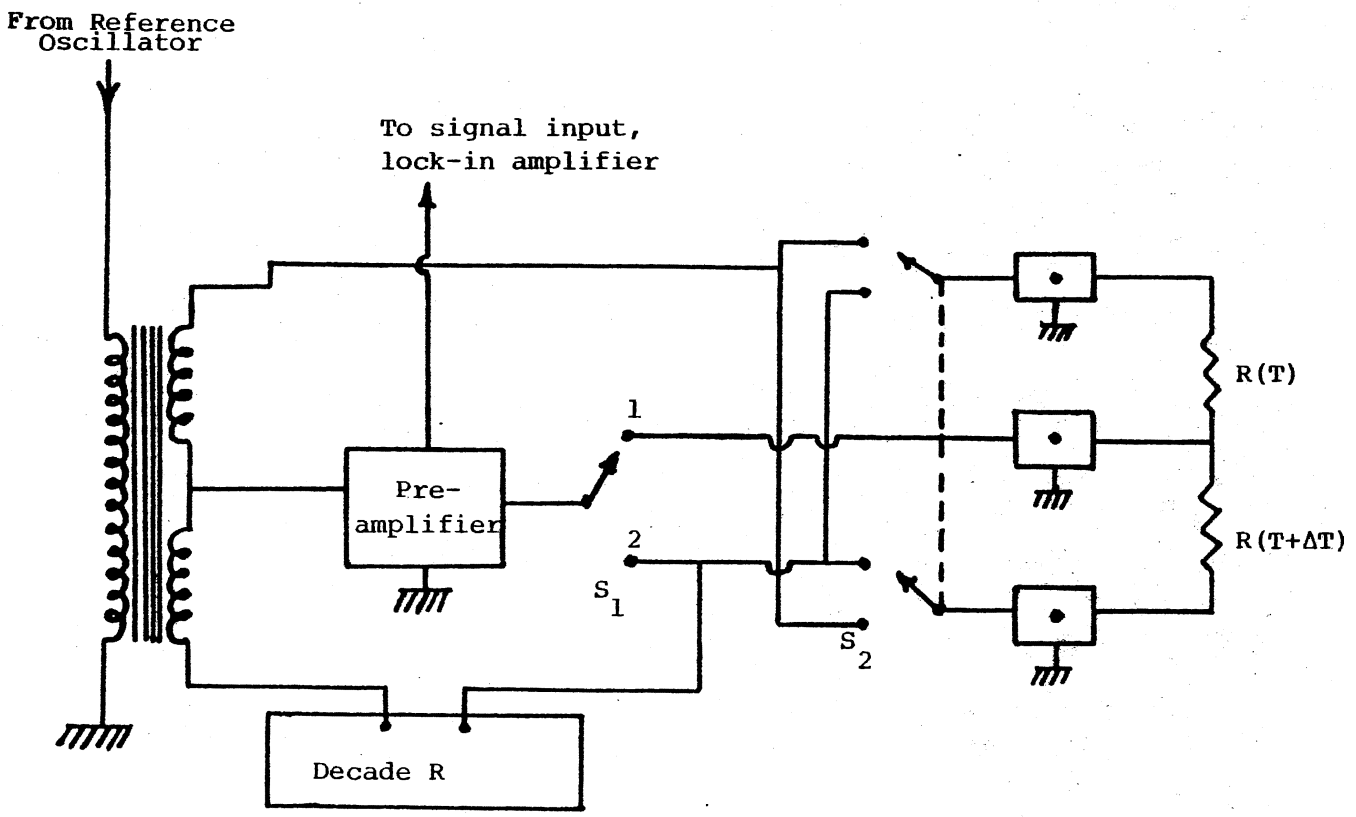

Figure 8. Resistance Bridge Circuit for Measurement of R and ΔR. With switch S_1 in position 1, the series combination of two resistors can be measured. With S_1 in position 2 the bridge measures the difference, ΔR, between the two resistors. S_2 reverses the connections between the two resistors.

Samples

The material was pure Z growth synthetic quartz lumbered bars purchased from Sawyer Research Products, Eastlake, Ohio. All thermal conductivity samples were cut from the lumbered bars for heat flow in the Y direction. The measurements were made on two different grades of crystals. One electronic grade sample labeled EG-S was measured. Two premium Q samples were measured, one from bar PQ-E and the other from bar PQ-S. Bar PQ-E has been extensively studied by the Oklahoma State University quartz project. Samples EG-S and PQ-S were measured in the as-received conditions and after a room temperature irradiation. Sample PQ-E was measured in the as-received condition from 1.5K to 48K and after a room temperature irradiation from 1.5K to 45K. Following the irradiation sample PQ-E was electrolyzed to replace the alkalis with hydrogen. The thermal conductivity was then run from 1.5K to 13K. Table I gives the sample dimensions and the aluminum content as estimated from the 3367 cm^{-1} and 3306 cm^{-1} infrared bands (4).

Measurements

The thermal conductivities of the samples were measured by the steady-state heat flow method (48). From Equation 22 and Figure 2, we see that to measure λ, we need to determine, A, ΔX, ΔT and $\dot{Q}$. A 30-40 ohm heater was wound on one end of the sample and cemented in place which GE varnish. The thermocouples and carbon resistors were attached to the sample with small clamps as described above. The sample was then clamped in the holder designed for the desired temperatures range. The holder was pumped out to better than 10^{-5} Torr after it was placed in the dewar. Then liquid nitrogen was introduced into the outer

TABLE I

SAMPLE SIZE, THERMOCOUPLE SEPARATION DISTANCE AND CONCENTRATION OF ALUMINUM FOR THE THERMAL CONDUCTIVITY SAMPLES

Sample	a(cm)	b(cm)	Δx(cm)	$N_{A\ell}$(10^{16} cm^{-3})
EG-S	.251	.300	1.05	10
PQ-S	.150	.275	1.40	2
PQ-E11	.358	.295	2.58	30

chamber and helium exchange gas into the inner chamber. A small amount of helium gas was also introduced into the heat leak chamber. After the sample's temperature has reached liquid nitrogen temperature, liquid helium was transferred into the inner dewar. With a good vacuum in the sample can, the gradient heater was turned on. When thermal equilibrium was reached T and ΔT were determined by measuring the thermocouple emf's. $\dot{Q}$ was determined by measuring the gradient heater current and voltage. Then with power off in the gradient heater, the power turned on the ambient heater to raise the temperature of the sample to the T; at this moment the measurement of the T and ΔT were repeated. T was found from the appropriate table which was constructed by Wolf (51) and Martin (52). ΔT was calculated from

$$\Delta T = \frac{[\varepsilon(on) - \varepsilon(off)]}{\frac{d\varepsilon}{dT}} \tag{23}$$

The procedure was the same for helium pot system except that here the resistances of carbon resistor thermometers were measured instead of the emf of thermocouples. A previously calibrated Germanium resistance thermometer which was attached to the pot was used to calibrate the Allen-Bradley resistors. ΔT was calculated from

$$\Delta T = \frac{[R(on) - R(off)]}{\frac{dR}{dT}} . \tag{24}$$

The calibration procedure will be discussed below.

Thermometry

For the temperature range of 3.5 to 140K, the temperature was de-

by a chromel versus gold-0.07 atomic percent iron thermocouple. Because of the high thermopower of gold-0.07 atomic percent iron for the temperature range 3.5 to 30K it was used as the negative element. On the other hand, chromel was used as the positive element because of its high positive thermopower for higher temperatures. These two elements gave excellent sensitivity for the entire temperature range of 3.5 to 140^{o}K.

Since the characteristic of each spool of wire used in the thermocouple might vary from one spool to the next, it was necessary to calibrate our thermocouple versus a calibrated thermometer. The chromel versus gold-0.07 atomic percent iron thermocouple was compared with a commercially calibrated Germanium resistance thermometer over the 3.5K to 20K range. For higher temperatures the table constructed by M. Wolf (51) and J. Martin (52) was used. They have calibrated the thermocouple against a platinum resistance thermometer. To determine $\frac{dE}{dT}$ for the entire range of temperature 3.5K to 140K the same table was used.

For the temperature range 1.5 to 4, a carbon resistance thermometer was used. The thermometers were commercial, 47 ohms, 0.1 watts Allen-Bradley Company resistors. We determine R versus T at this range of temperature by comparing with a calibrated Germanium resistor mounted on the helium pot. We found that the equation

$$\log R = a+b\left[\frac{\log R}{T}\right]^{\frac{1}{2}} \tag{25}$$

suggested by Rose-Innes (49) fit the data. Plot of log R versus $\left[\frac{\log R}{T}\right]^{\frac{1}{2}}$ gives a straight line from which we can determine a and b. To determine $\frac{dR}{dT}$, following relation was used.

$$\frac{dR}{dT} = -\frac{R}{b^2}\left[\frac{(\log R-a)^3}{\log R+a}\right] \tag{26}$$

This procedure was repeated in each run because there was a possibility that irradiation and thermal cycling might change the characteristic value of carbon resistors. In the temperature range 1.64K to 4.22K these resistors had extremely high sensitivities, ranging from 2600 ohms per degree at 1.64 to 130 ohms per degree at 4.22K.

Errors

Equation (22) was used to find thermal conductivity. The sample cross section, input power, thermometer separation, sample temperature and gradient temperature should be considered as possible sources of error. The cross-sectional area, A = axb (a = 0.358 cm, b = 0.295 cm), was determined by measuring a and b with a vernier caliper to the nearest 0.05 mm. Consequently there was approximately a 3% error in measuring the area. In samples which were not a perfect parallelpiped the average values were used. The measurement of the thermometer spacing, L, was the most uncertain geometrical measurement taken. It was made by measuring the distance between the centers of the thermometer clamps with a vernier caliper. The measurement of cross-section and the thermometer spacing was the same for set of data for a sample so the uncertainities in these measurements remained constant and did not affect the shape of the thermal conductivity curve.

The relation P = VI was used to determine the input power. The current I was determined by measuring the voltage drop across a 10 ohm standard resistor, read with a digital millivoltmeter. The voltage V was also read directly on the digital millivoltmeter. Both I and V were

read to four figures and all the measurements had an uncertainty of approximately ±3 in the fourth digit which will lead to the maximum error in the input power to be about 1%. The relative uncertainty between data points, however, should have been much smaller since the meter's errors would be in the same direction and should have approximately the same magnitude for each determination.

In the determination of T, two elements must be considered: first the error in the K-3 potentiometer which was used to determine the emf, and second, errors in the calibration. The K-3 potentiometer measures the voltage to ±.5 microvolt, which is corresponds to .02% error in emf at 4.2K which is very small, but combined with other possible errors in calibration, thermal emf's in wires, switches and connectors, will correspond to a maximum temperature uncertainty of 50 mK to 28 mK at 77K. The relative uncertainty between data points and data runs, however, was considerably less than the total maximum errors given above. The reproducibility of the thermocouples was better than 0.02% on successive cool-downs (53).

For measurement of ΔT, we typically observed an emf of 0.5 to 1.0 microvolt on the Honeywell potentiometer. The resolution of the Honeywell potentiometer is 0.01 microvolt which will lead us to about 2% error. On the other hand the possible error in table for $\frac{dE}{dT}$ is about 3% (52) so we can say ΔT is good to about 4-5 percent.

At low temperatures ($T \leq 4.2K$) where the carbon resistors were used the following errors should be considered; the measurement of the resistance of the carbon and germanium resistors were made at temperature T, and this temperature was determined from a graph of resistance of the germanium resistance thermometer versus temperature. The accuracy of

this graph was about 1.5% at 1.6K to 0.6% at 4.2K. This germanium resistor had previously been calibrated against a commercial germanium resistor with accuracy ±5 mK at 1K to 5K. Equation (25) as determined by the straight line drawn through the calibration data for carbon resistor had a standard derivation of 1.6%. The ac-bridge with the lock-in-amplifier null detector was able to resolve 0.1 ohm; thus, we could resolve the temperature to within about 0.005% over the 1.5K to 4.2K range. From this information we can estimate a 2 to 3 percent error when using the carbon resistance thermometers.

CHAPTER IV

RESULTS AND DISCUSSION

The thermal conductivities (with heat flow parallel to the Y) axis of three different synthetic quartz samples were measured. The shape of the thermal conductivity curves for all three as-received, Electronic grade sample, EG-S and Premium Q samples (PQ-S and PQ-E11) were characteristic for single crystal insulating materials as Figure 9 shows. For temperatures above the thermal conductivity maximum temperature, the thermal conductivities for all three samples were almost the same, and they had the characteristic slope of T^{-1}. Therefore, phonon-phonon scattering dominates at these higher temperatures. Although the thermal conductivity of sample EG-S agrees with that of sample PQ-E11 at the higher temperature it is much lower than that of the Premium Q sample at low temperatures. This reduced thermal conductivity is probably caused by the larger impurity and defect content of Electronic grade material. The Premium Q sample PQ-E11 has a maximum thermal conductivity approximately one-half of that reported by Zeller and Pohl (12) and by Wasim and Nara (13) for natural quartz. Only sample PQ-E11 was measured at temperatures lower than 5K, the thermal conductivity curve had a slope of T^3.

The solid curves through the data for the as-received samples shown in Figure 9 obtained from a theoretical fit to the data with the Debye-Callaway expression (25), for the thermal conductivity, λ,

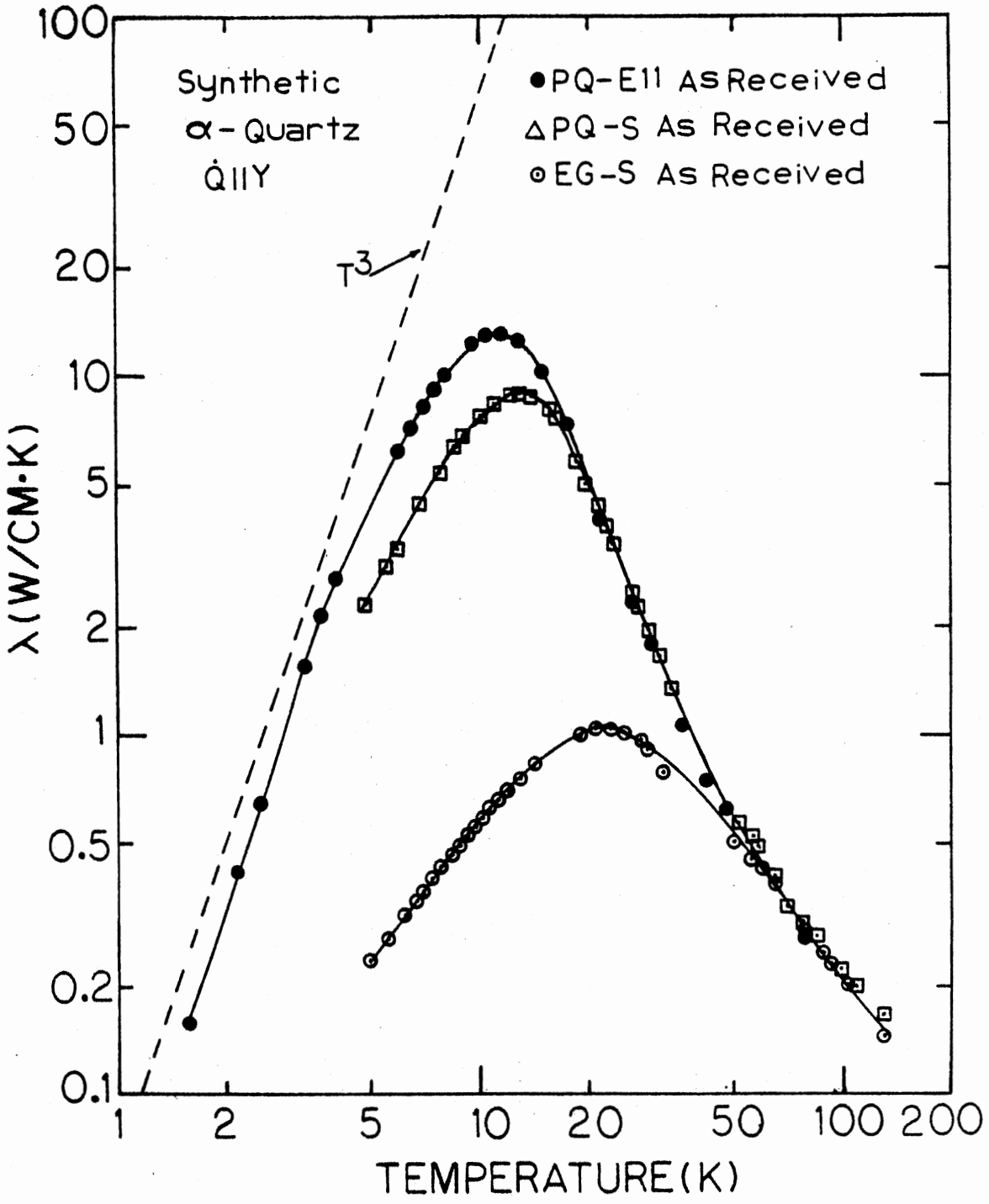

Figure 9. Low Temperature Thermal Conductivity of EG-S, PQ-S, and PQ-E11 Samples As-Received

$$\lambda = \frac{k}{2\pi v}\left(\frac{kT}{\hbar}\right)^3 \int_0^{\theta/T} \tau\, x^4\, e^x (e^x-1)^{-2}\, dx \qquad (27)$$

In this expression, $x = \hbar\omega/kT$, ω is the phonon frequency, v is the average sound velocity, θ is the Debye temperature, and τ is the combined relaxation time for the phonon scattering processes. The inverse relaxation time was taken as

$$\tau^{-1} = \frac{v}{L} + A\omega^4 + (B_1 + B_2\, e^{-\theta/\alpha T})\omega^2 T \qquad (28)$$

where the three terms represent boundary, point defect and phonon-phonon scattering. The Debye temperature, θ, was taken to be 470K (54). The average sound velocity was calculated to be 4.97×10^5 cm/sec using the relation

$$\frac{1}{v} = \frac{1}{3}\left(\frac{1}{v_\ell} + \frac{2}{v_t}\right) \qquad (29)$$

where the transverse and longitudinal sound velocities were $v_t = 4.66 \times 10^5$ cm/sec and $v_\ell = 5.73 \times 10^5$ cm/sec. The parameters L, A, B_1, B_2 and a were adjusted to fit Eq. 1 to the experimental value. The parameters used are given in Table II. Using following equation

$$L = 2\pi^{-\frac{1}{2}}(a \cdot b)^{\frac{1}{2}} \qquad (30)$$

for sample PQ-E11 boundary scattering parameter, L, was found to be very close to the actual dimensions. The point defect term, A, for this sample was lightly smaller than the value $A = 7.94 \times 10^{-46}$ estimated for isotope scattering. For sample, EG-S, both the boundary scattering strength and the point defect scattering strength had to be greatly in-

TABLE II

ADJUSTABLE PARAMETERS FOR FITTING THE THEORETICAL RESULT WITH EXPERIMENTAL DATA

PQ-E11 Sample	L(cm)	A(sec^3)	$B_1(\frac{sec}{K})$	$B_2(\frac{sec}{K})$	a	$\omega_o(\frac{rad}{sec})$	$F(\frac{rad^2}{sec})$
Theoretical	.367[†]	7.94×10^{-46}[#]	-----	-----	-	-----	-----
As-Received	.278	4.7×10^{-45}	4.4×10^{-21}	4.6×10^{-18}	6	0.0	0.0
Irradiated	.278	2.7×10^{-45}	4.4×10^{-21}	4.6×10^{-18}	6	2.75×10^{12}	2.9×10^{-15}
Swept	.325	3.4×10^{-46}	1.4×10^{-21}	4.6×10^{-18}	6	2.75×10^{12}	2.9×10^{-15}

[†]Calculated from Equation (30).

[#]Calculated in Appendix A.

creased.

The Electronic Grade sample, EG-S, and the Premium Q sample, PQ-S, were irradiated for 4 minutes at room temperature with a 5μA current of 1.5 MeV electrons. As shown in Figure 10 no significant change was observed in the thermal conductivity. But when sample PQ-E11 was irradiated at room temperature to the same dose a dip centered near 5K was introduced into its thermal conductivity as shown in Figure 11. Wasim and Nava (13) observed a similar dip after irradiation in the thermal conductivity of natural quartz. Recent EPR investigations by Markes and Halliburton (5), IR investigations by Sibley et al. (4) and acoustic loss investigation by Doherty et al. (55) have shown that when as-received unswept synthetic quartz is irradiated at room temperature the alkali ion which was providing change compensation for substitutional aluminum is removed from the aluminum site and is replaced by either a proton on a hole on an adjacent oxygen to form the Al-OH center or the $[Al_{e+}]^{o}$ cen-er. The relative concentrations of Al-OH and $[Al_{e+}]^{o}$ centers is determined by the number of deep electron traps. (If the sample is subsequently irradiated at temperatures near 77K all of the Al-OH centers can be converted to $[Al_{e+}]^{o}$ centers; the Al-OH centers recover upon warming to 300K). Since either the Al-OH or $[Al_{e+}]^{o}$ centers might cause a resonant phonon scattering we have included a resonant term of the form

$$\tau_r^{-1} = \frac{FW^2}{(\omega^2 - \omega_o^2)^2} \tag{31}$$

in the combined relaxation time (Equation 5). This resonant form has been used by Pohl (46) to analyze local mode scattering in alkali

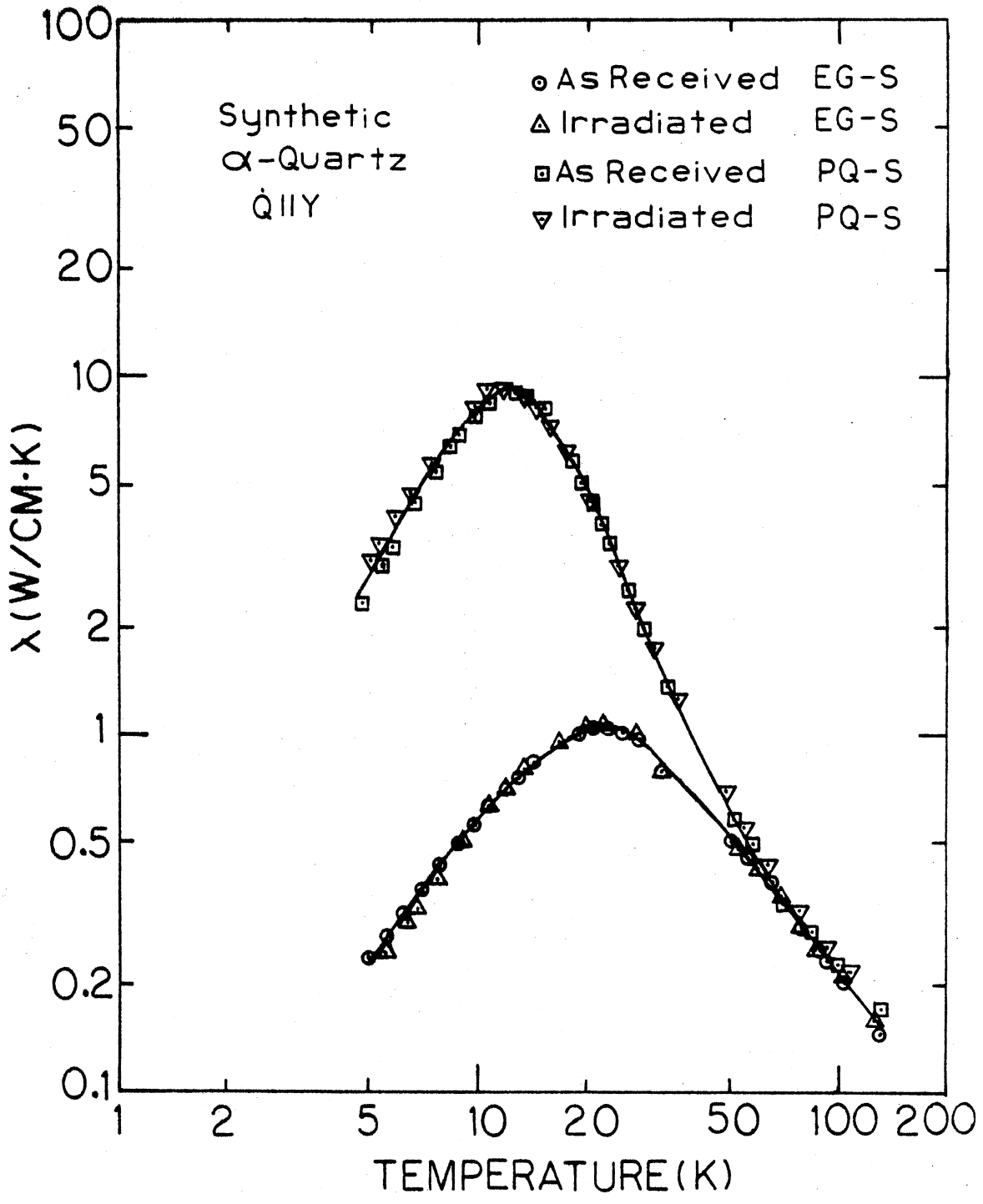

Figure 10. Low Temperature Thermal Conductivity of EG-S and PQ-S Samples As-Received and Irradiated

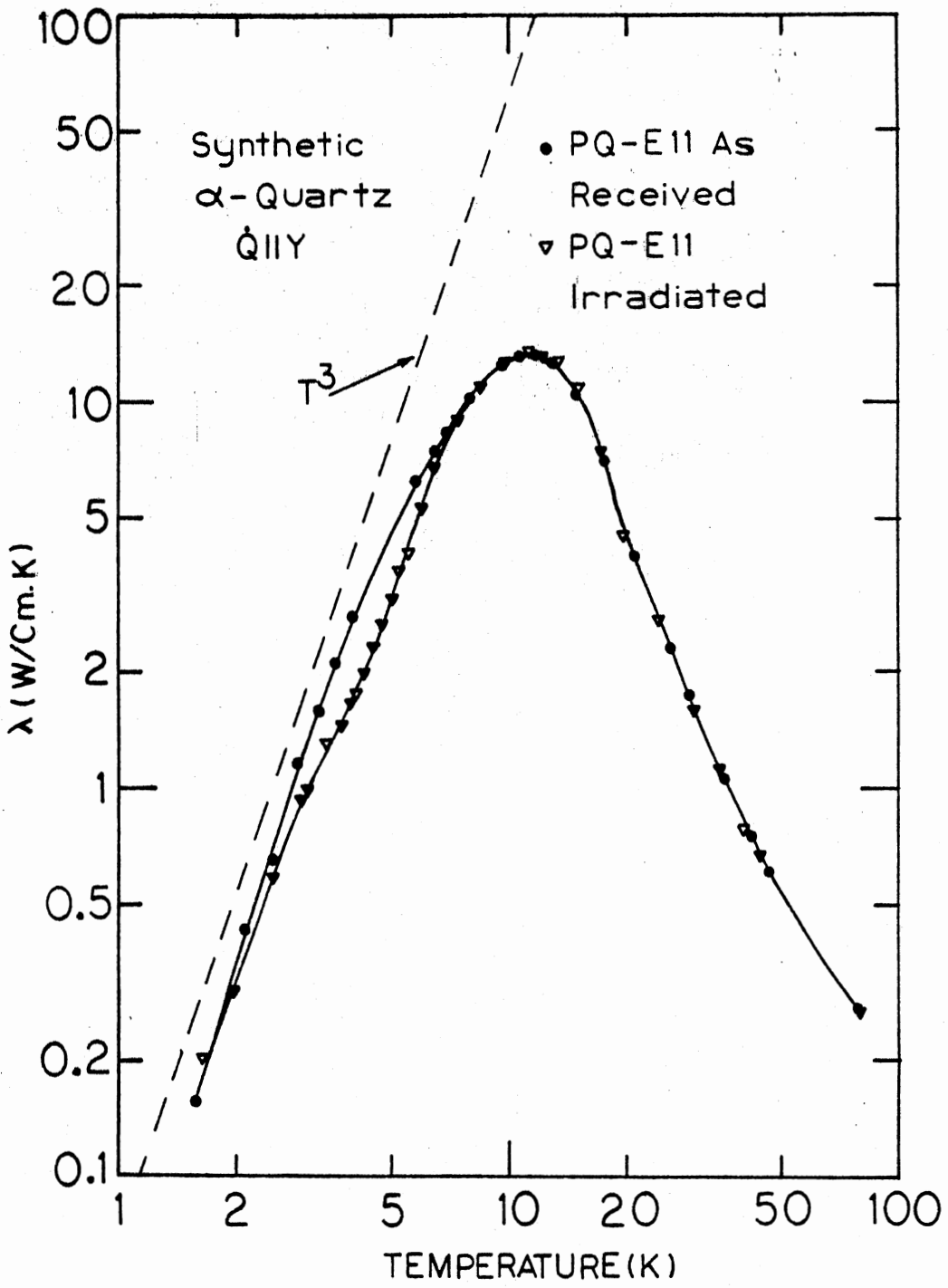

Figure 11. Low Temperature Thermal Conductivity of PQ-E11 Sample As-Received and Irradiated

halides. Figure 11 compares the results for sample PQ-E11 in the as-received and irradiated condition. Figure 12 shows λ/T^3 versus T for sample PQ-E11 in the as-received condition and after irradiation. The curve drawn through the results for the irradiated sample was calculated with $\omega_o = 2.7 \times 10^{12}$ rad/sec^{-1} and $F = 2.9 \times 10^{-15}$ rad^2/sec. These values are included in Table II.

In order to determine whether the resonant scattering was caused by the Al-OH center or by the $[Al_{e+}]^o$ centers, sample PQ-E11 was electrolyzed in a hydrogen atmosphere. This electrolysis or sweeping removes the alkali and replaces them with hydrogen to form the Al-OH center. The $[Al_{e+}]^o$ centers would also be removed. After sweeping in hydrogen the sample was replaced in the thermal conductivity apparatus and run over the 1.5K to 13K range. Figure 13 compares the results for sample PQ-E11 in the as-received and swept condition. Sweeping has increased the thermal conductivity maximum from 13 W/cmK to 23 W/cmK. This large increase is probably caused by the removal of the alkalis from the sample. The resonant dip near 5K is still present in the sample. Figure 14 shows λ/T^3 versus T for sample PQ-E11 in the as-received and swept condition. Figure 15 shows λ/T^3 versus T for sample PQ-E11 in the irradiated and swept condition. The curve through results for the sample after sweeping was also calculated with an $\omega_o = 2.7 \times 10^{12}$ rad/sec^{-1} in Equation (3). The value for F is given in Table II. Since the $[Al_{e+}]^o$ centers and the alkalis which might be clustered after irradiation are not present after sweeping the resonant scattering is most likely caused by the Al-OH centers.

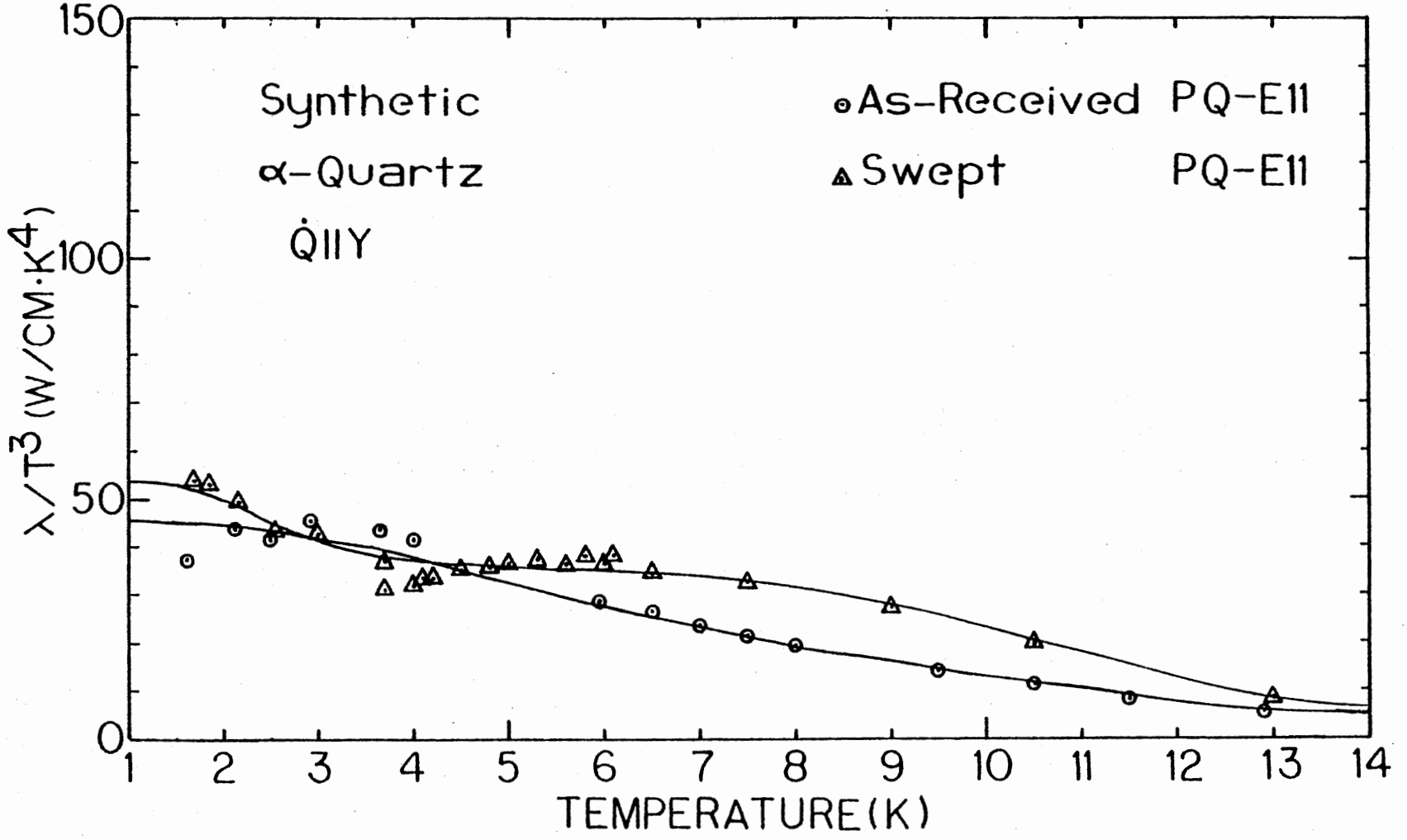

Figure 12. Comparing λ/T^3 Versus T for PQ-E11 Sample, As-Received and Irradiated

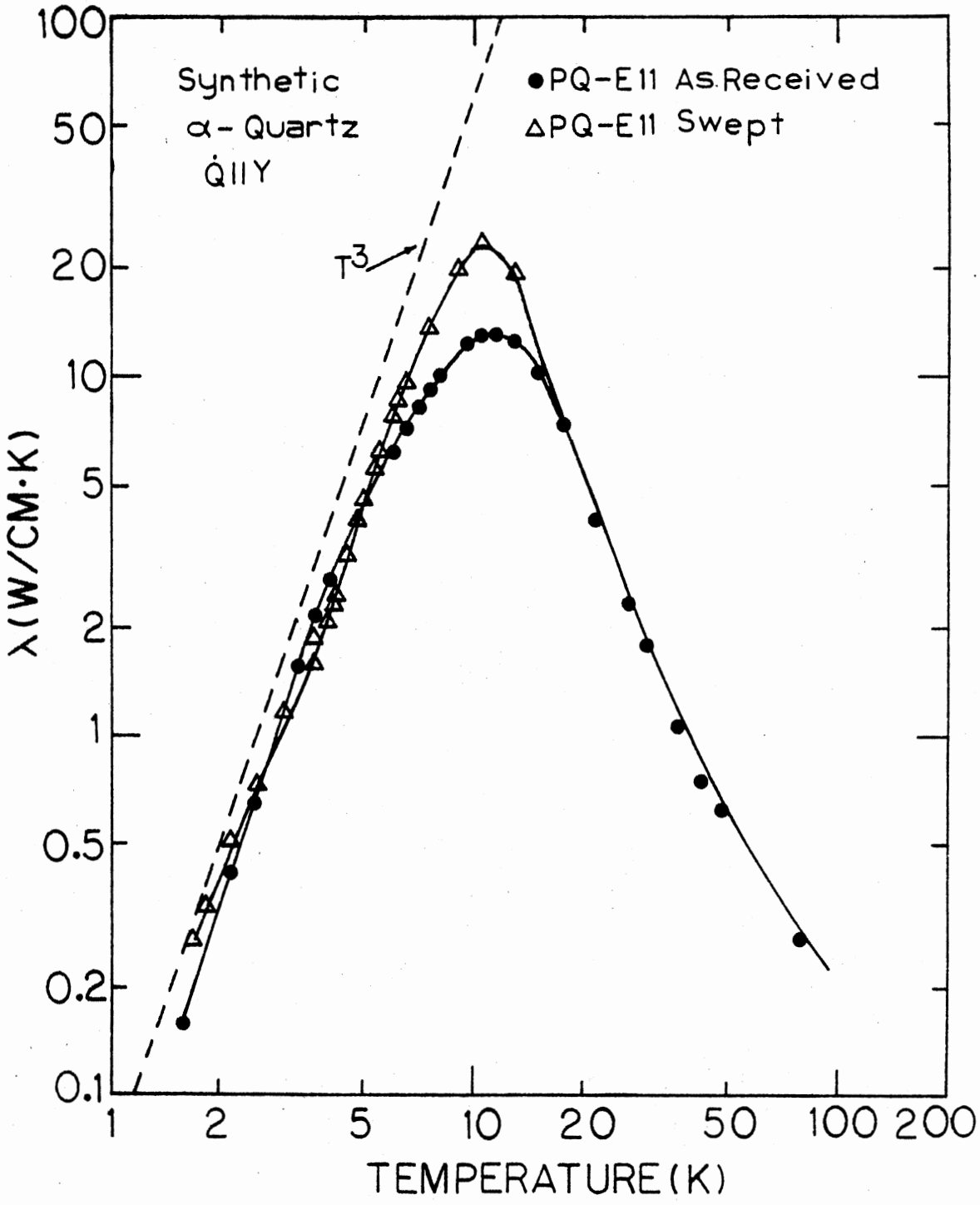

Figure 13. Low Temperature Thermal Conductivity of PQ-E11 Sample As-Received and Swept

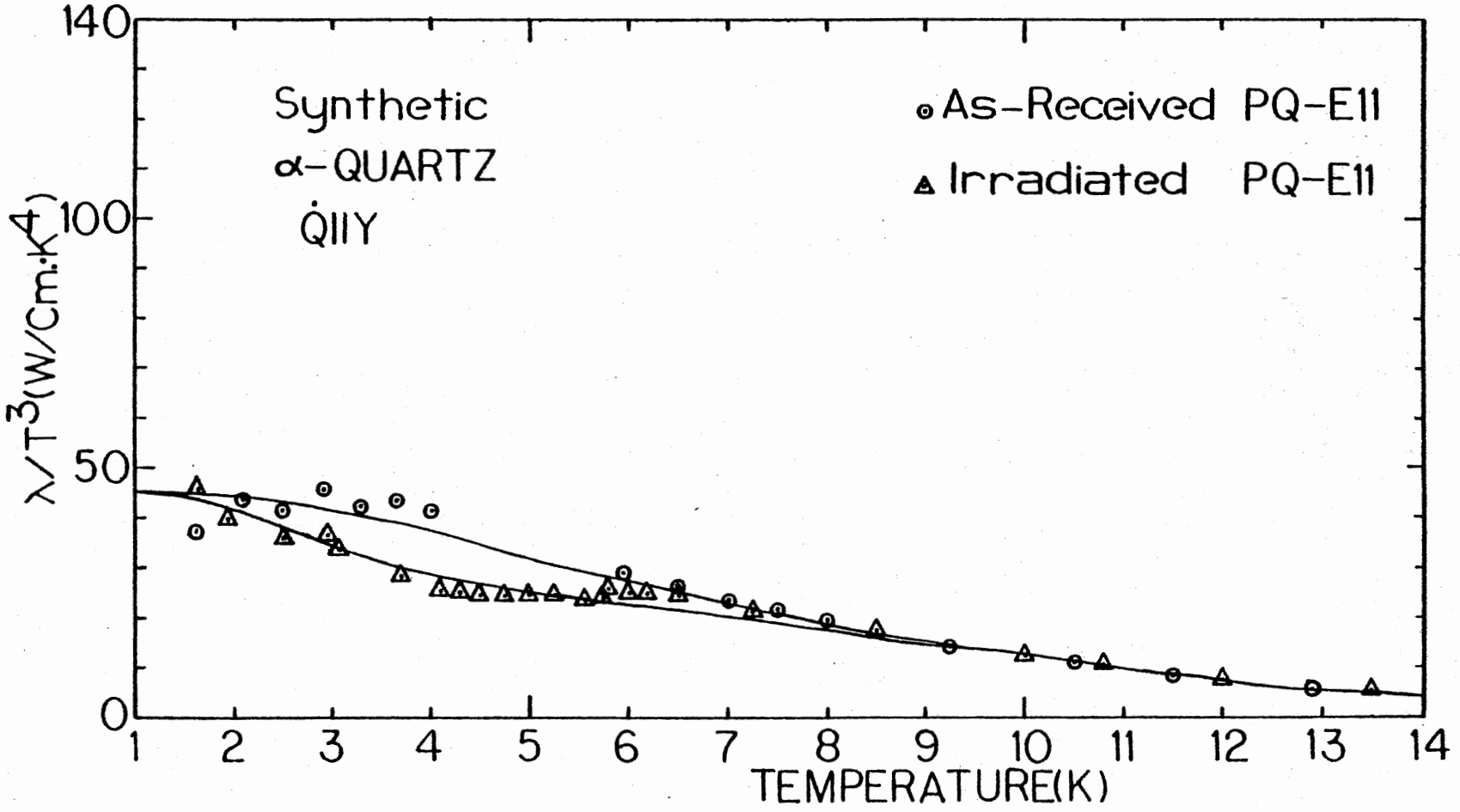

Figure 14. Comparing λ/T^3 Versus T for PQ-E11 Sample As-Received and Swept

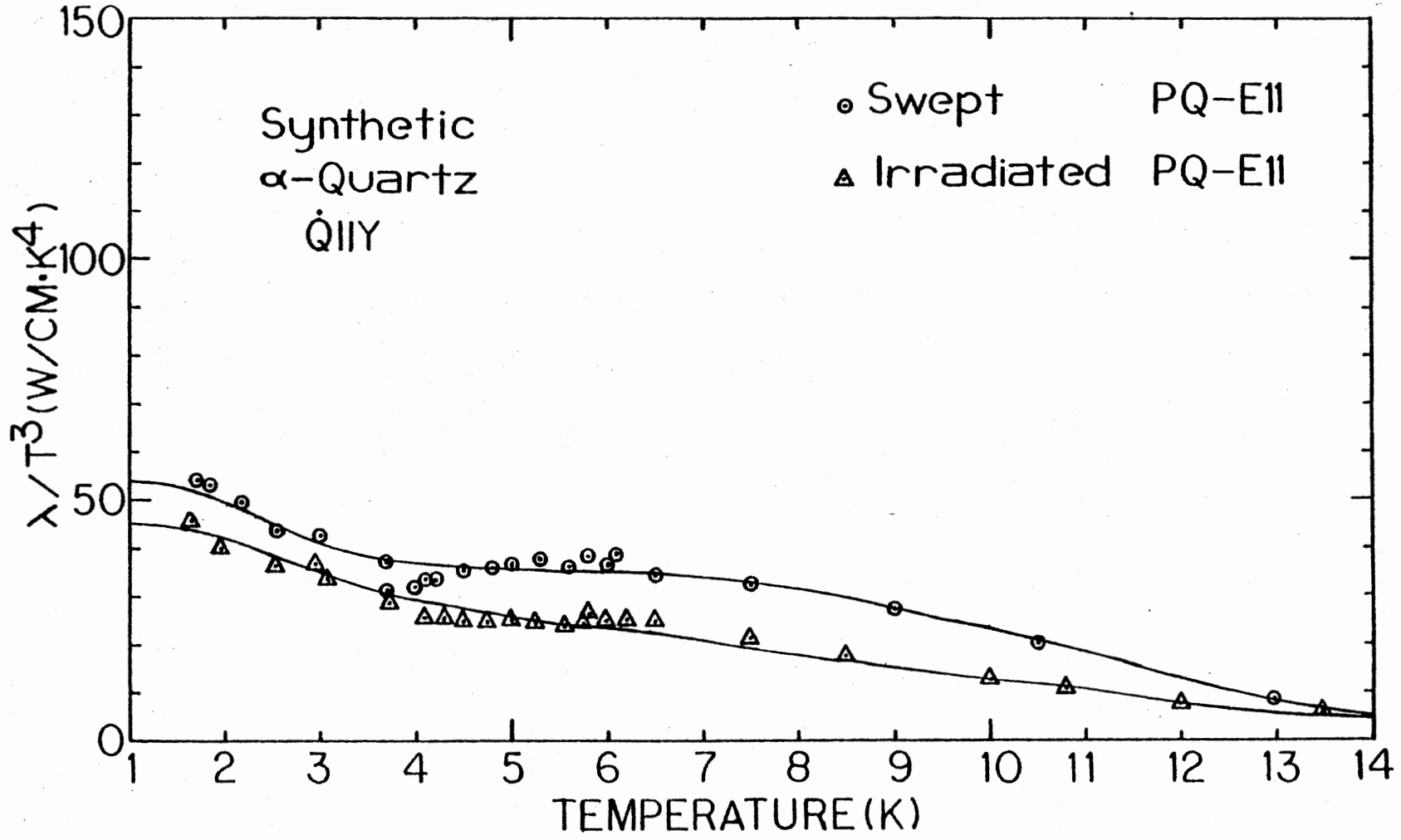

Figure 15. Comparing λ/T^3 Versus T for PQ-E11 Sample Irradiated and Swept

CHAPTER V

SUMMARY

The thermal conductivities of several synthetic quartz samples were measured. The shape of the thermal conductivity curves were characteristic for single crystal insulating material. The maximum thermal conductivity (PQ-E11 sample) was found to be approximately one-half of that reported by Zeller and Pohl (12) and by Wasim and Nava (13) for natural quartz. Irradiation of samples EG-S and PQ-S at room temperature did not cause significant differences with the thermal conductivity of as-received samples. For PQ-E11 a dip centered near 5K was introduced into its thermal conductivity after it was irradiated at room temperature. This result suggested that either the Al-OH or $[Al_{e+}]^{o}$ centers have caused a resonant phonon scattering. In order to determine whether the resonant scattering was caused by the Al-OH centers or by the $[Al_{e+}]^{o}$ centers, sample PQ-E11 was electrolyzed in hydrogen, this sweeping removed the alkalis and replaced them with hydrogen to form the Al-OH centers and also $[Al_{e+}]^{o}$ centers were removed. The maximum thermal conductivity was then observed to be higher, because of removal of alkali and $[Al_{e+}]^{o}$ centers. The dip near 5K was still present, which indicated the resonant scattering is most highly have been caused by the Al-OH centers.

Future Work

The dose dependence of the irradiation induced resonant scattering should be investigated. Irradiation of a swept sample at 77K will replace all of the Al-OH centers with $[Al_{e+}]^{o}$ centers and, therefore, should remove the 5K resonance. Sweeping the sample in deuterium would replace the Al-OH centers with Al-OD centers. This should lower the resonant frequency of the scattering. Sweeping lithium or sodium into a sample would also be interesting.

BIBLIOGRAPHY

1. Hurlbut, C. S., Manual of Minerology (19th Edition), John Wiley and Son, Inc. (1977).

2. Deer, W., R. Hamie and J. Zussman, An Introduction to the Rock Forming Minerals, London, Longmans (1966).

3. Laudise, A. and J. W. Nielson, Solid State Physics, 12, Editors F. Seitz and D. Turnbull, Academic Press (1961).

4. Sibley, W. A., J. J. Martin, M. C. Wintersgill and J. D. Brown, J. Appl. Phys. 50(8), 5449 (1979).

5. Markes, M. E. and L. E. Halliburton, J. Appl. Phys. 50(12), 8172 (1979).

6. King, J. C., Bell System Tech. J., 38, 573 (1959).

7. Kats, A., Philips Res. Rep. 17, 133 (1962).

8. Fraser, D. B., J. Appl. Phys. 35, 2913 (1964).

9. Capone, B. R., A. Kahan, R. N. Braun and J. R. Buckmelter, IEEE Trans. on Nuc. Sci. NS-17, 217 (1970).

10. Berman, R., Royal Society of London, A208, 90 (1951).

11. Fraser, D. B., Physical Acoustic, edited by W. P. Mason, Vol. 5, pp. 59-110, Academic Press, New York (1968).

12. Zeller, R. C. and R. O. Pohl, Physical Review B, 4, No. 6, 2029 (1971).

13. Wasim, S. and R. Nava, Phys. Stat. Sol(a) 51, 359 (1979).

14. Halliburton, L. E., M. Markes, J. J. Martin, S. P. Doherty, N. Koumvakalis and W. A. Sibley, IEEE Trans. on Nuc. Sci., NS-26, No. 6, 4851 (1979).

15. Martin, J. J., S. P. Doherty, L. E. Halliburton, M. Markes, N. Koumvakalis and W. A. Sibley, Proceedings of the 33rd Annual Symposium on Frequency Control, 1979.

16. Klemens, P. G., Solid State Physics 7, edited by F. Seitz and D. Turnbull, Academic Press, New York (1958).

17. Klemens, P. G., Encyclopedia of Physics 14, 198, edited by S. Flugge, Springer-Verlag, Berlin (1956).

18. Carruthers, P., Rev. Mod. Phys. 33, 92 (1961).

19. Ziman, J. M., Electrons and Phonons, Clarendon Press, Oxford (1960).

20. Debye, P., Vorbrage Uberdie Kinetische Theorie der Materie and der Electrizitat (1914).

21. Peierls, R. E., Ann. Physik, 3, 1055 (1929).

22. Klemens, P. G., Proc. Phys. Soc. 68, 1113 (1955).

23. Klemens, P. G., Proc. Roy. Soc. A208, 108 (1951).

24. Peierls, R. E., Quantum Theory of Solids, Clarendon Press, Oxford (1955).

25. Callaway, J., Phys. Rev. 113, 1046 (1959).

26. de Haas, W. J. and Th. Biermasz, Physica 2, 673 (1935).

27. Casimir, H. B. G., Physica 5, 495 (1938).

28. Berman, R., E. L. Foster, and J. M. Ziman, Proc. Roy. Soc. A231, 130 (1955).

29. Tacher, P. D., Phys. Rev. 156, 975 (1967).

30. Holland, M. G., and L. J. Neuringer, Proc. Internatl. Conf. on Physics of Semiconductors, 474 (1962).

31. Berman, R., F. E. Simon, and J. M. Ziman, Proc. Roy. Soc. A220, 171 (1953).

32. Slack, G. A., Phys. Rev. 105, 832 (1957).

33. Walton, D., Phys. Rev. 135, A753 (1964).

34. Worlock, J. M., Phys. Rev. 147, 636 (1966).

35. Pohl, R. O., Phys. Rev. 118, 1499 (1960).

36. Carruthers, J. A., J. F. Cochran, and K. Mendelssohn, Cryogenics 2, 160 (1962).

37. Walton, D., Phys. Rev. B1, 1234 (1970).

38. Huber, D. L., Phys. Lett. 20, 230 (1966).

39. Walker, C. T. and R. O. Pohl, Phys. Rev. 131, 1433 (1963).

40. Rayleigh, Lord (1896), Theory of Sound (2nd edn.), 2, Dover Publications, New York (1945).

41. Slack, G. A., Phys. Rev. 126, 427 (1962).

42. Herring, C., Phys. Rev. 95, 954 (1954).

43. Wolf, M. W. and J. J. Martin, Phys. Stat. Sol.(a) 17, 215 (1973).

44. Martin, J. J., J. Phys. Chem. Solids, 33, 1139 (1972).

45. Hartmann, J. B. and J. J. Martin, Phys. Stat. Sol.(b) 84, 721 (1977).

46. Pohl, R. O., Phys. Rev. Lett. 8, 481 (1962).

47. Walker, C. T. and R. O. Pohl, Phys. Rev. 131, 1433 (1963).

48. Berman, R., Thermal Conduction in Solids, Clarendon Press, Oxford (1976).

49. Rose-Innes, A. C., Low Temperature Laboratory Techniques, 2nd edn., The English Universities Press, Ltd. (1973).

50. White, G. K., Experimental Techniques in Low-Temperature Physics, 2nd edn., Clarendon Press, Oxford (1968).

51. Wolf, M. W., Unpub. Ph.D. Thesis, Oklahoma State University (1974).

52. Martin, J. J., private communication (1979).

53. Finnemore, D. K., Rev. Sci. Instr. 36, 1364 (1965).

54. Jones, G. H. S., and A. C. Hallis-Hallett, Can. J. Phys. 38, 696 (1960).

55. Doherty, S. P., J. J. Martin, A. F. Armington, and R. N. Brown, J. App. Phys. (to be published).

A P P E N D I X

APPENDIX A

THE CALCULATION OF THE PARAMETER A FOR ISOTOPE POINT DEFECT SCATTERING IN SiO_2

Atomic weight of oxygen: 15.9994 gm

Atomic weight of silicon: 28.086 gm

Density of SiO_2: 2.65 gm/cm^3

Molecular weight of SiO_2: 60.08 gm

Molecular volume of SiO_2: $V = (\frac{60.08}{2.65}) \cdot \frac{1}{6.02 \times 10^{23}} = 3.76 \times 10^{-23}$ cm^3

Velocity of sound in SiO_2: $v = 4.97 \times 10^5$ cm/sec and $\delta = 3\sqrt{V} = 3\sqrt{3.76 \times 10^{-23}} = 3.35 \times 10^{-8}$.

Oxygen Isotopes:

Atomic Mass(M)	Natural Abundance (f_i)
16	99.76% = .9976
18	.204% = .0204
17	.039% = .00039

Silicon Isotopes:

Atomic Mass(M)	Natural Abundance (f_i)
28	92.28% = .0228
29	4.67% = .0467
30	3.09% = .0305

$$\Gamma = \Sigma \frac{X}{x+y+\ldots} \left(\frac{M_A}{\bar{M}}\right)^2 \Gamma_A + \frac{Y}{x+y+\ldots} \left(\frac{M_B}{\bar{M}}\right) \Gamma_B + \ldots$$

where

$\Gamma_A = \Sigma_i f_i \left(\frac{\Delta M_i}{M_A}\right)^2, \ldots$ f_i = Natural Abundance and for SiO_2

x = 1, y = 2 (represent one silicon and two oxygen)

$$\Gamma_{S_i} = \sum_i f_{S_i i} \left(\frac{\Delta M_{S_i i}}{M_{S_i}}\right)^2 \quad \text{where } i = 28, 29, 30$$

$$= (0.9228)\left(\frac{0.086}{28}\right)^2 + (0.0467)\left(\frac{.914}{29}\right)^2 + (0.0305)\left(\frac{1.914}{30}\right)^2 = 1.79 \times 10^{-4}$$

$$\Gamma_o = \Sigma_i f_{o,i} \left(\frac{\Delta M_{oi}}{M_o}\right)^2 \quad \text{where } i = 16, 17, 18$$

$$= (0.9976)\left(\frac{.0006}{16}\right)^2 + (0.00039)\left(\frac{1.0006}{17}\right)^2 + (0.0204)\left(\frac{2.0006}{18}\right)^2 = 2.53 \times 10^{-4}$$

then

$$\Gamma_\bullet = \frac{1}{3}\left(\frac{15.9994}{60.08}\right)^2 \cdot 2.53 \times 10^{-4} + \frac{2}{3}\left(\frac{28.086}{60.08}\right)^2 \cdot 1.79 \times 10^{-4} = 3.2 \times 10^{-5}$$

and

$$A = \frac{\delta^3 \Gamma}{4\pi v^3}$$

$$= \frac{(3.35 \times 10^{-8})^3 \cdot 3.2 \times 10^{-5}}{4\pi (4.97 \times 10^5)^3}$$

$$= 7.94 \times 10^{-46} \text{ sec}^3$$

APPENDIX B

TABULATION OF DATA FOR SAMPLE EG-S (AS-RECEIVED)

HEAT LEAK APPARATUS (3.5 to 140K) - L/A = 13.98

Temperature (K)	Thermal Conductivity (mW/Cm·K)	Power Input (mW)	ΔT (K)
140.0	145	1.8	.168
120.0	176	1.7	.138
115.0	203	1.7	.122
94.5	232	1.7	.105
89.2	256	6.0	.331
88.5	249	1.7	.096
78.0	290	5.1	.242
65.5	365	1.7	.065
64.0	406	1.7	.058
60.0	424	1.9	.055
59.0	433	1.7	.054
56.0	456	1.7	.051.
53.0	496	1.7	.047
50.5	505	1.6	.046
32.0	787	4.3	.070
30.7	890	4.3	.067
29.0	917	4.3	.065
28.0	977	4.4	.062
25.0	1010	4.2	.098
24.2	1044	4.3	.057
23.2	1045	4.3	.057
21.0	1031	4.3	.058
19.9	1018	4.3	.050
17.5	1027	5.7	.078
16.4	992	5.3	.070
15.3	926	5.5	.080
14.1	831	5.4	.090
13.0	749	5.7	.100
12.5	729	5.4	.090
12.4	724	7.8	.151
12.0	702	7.9	.156
11.6	674	7.8	.163
11.5	660	4.4	.090
11.2	648	7.9	.169

APPENDIX B (Continued)

Temperature(K)	Thermal Conductivity (mW/Cm·K)	Power Input(mW)	ΔT(K)
10.7	622	7.8	.176
10.3	589	7.9	.186
9.8	555	7.9	.198
9.3	526	7.9	.208
8.8	489	7.1	.200
8.4	461	7.1	.213
7.9	430	7.1	.229
7.4	398	6.3	.220
7.0	365	4.3	.160
6.7	347	5.6	.220
6.2	314	7.1	.300
5.6	270	4.3	.220
5.2	241	2.2	.125
5.0	236	2.2	.128

APPENDIX C

TABULATION OF DATA FOR SAMPLE EG-S (IRRADIATED)

Heat Leak Apparatus (3.5 to 140K) - L/A = 13.98

Temperature (K)	Thermal Conductivity (mW/Cm·K)	Power Input (mW)	ΔT(K)
142.6	154	6.0	.540
142.5	154	5.9	.530
137.5	160	5.9	.510
131.0	166	6.0	.500
111.0	196	5.9	.420
103.2	210	5.9	.390
94.7	229	6.0	.360
85.9	247	5.8	.329
83.2	255	6.0	.330
78	284	4.5	.220
76.5	287	4.5	.210
68.6	333	7.5	.310
68.0	334	6.1	.250
66.2	335	7.4	.300
63.4	353	4.9	.190
58.1	416	4.6	.150
54.4	441	4.6	.140
53.7	458	5.0	.150
51.7	478	4.8	.130
27.4	1003	4.7	.065
25.8	1039	4.7	.060
24.2	1047	4.3	.057
23.2	1079	4.3	.050
22.4	1089	4.4	.053
20.8	1090	4.5	.050
20.0	1064	4.5	.050
17.2	1016	4.4	.060
16.2	984	4.4	.060
16.1	951	4.4	.060
13.5	807	4.3	.074
11.7	676	4.1	.080
10.8	620	4.3	.096
9.8	549	4.3	.109
9.0	494	4.3	.120
7.7	391	4.2	.150

APPENDIX C (Continued)

Temperature (K)	Thermal Conductivity (mW/Cm·K)	Power Input (mW)	ΔT(K)
6.8	325	4.2	.180
6.4	300	4.2	.190
5.5	241	4.3	.240

APPENDIX D

TABULATION OF DATA FOR SAMPLE PQ-S (AS-RECEIVED)

Heat Leak Apparatus (3.5 to 140K) - L/A = 14.78

Temperature (K)	Thermal Conductivity (mW/Cm·K)	Power Input (mW)	ΔT(K)
147.0	161	5.8	.530
135.7	173	5.8	.490
123.8	182	5.8	.460
110.1	207	6.0	.440
100.1	228	5.9	.380
92.4	255	6.0	.340
87.7	271	6.0	.320
81.1	303	6.0	.290
79.1	309	6.0	.280
78.7	308	6.0	.289
71.1	340	4.7	.190
66.7	399	6.0	.220
63.0	438	4.6	.150
55.0	535	5.7	.150
52.6	585	6.4	.160
	L/A = 33.94		
66.2	414	8.4	.680
63.0	449	4.5	.330
59.2	500	5.1	.340
57	534	4.8	.300
52.5	584	7.7	.440
34.2	1376	7.8	.190
31.6	1676	7.7	.155
29.3	1997	7.3	.124
27.7	2275	7.5	.112
26.5	2514	8.0	.108
23.6	3477	6.9	.067
22.2	3759	5.9	.053
21.2	4401	5.9	.045
19.7	5011	5.9	.039
18.7	5837	5.9	.034
17.3	7173	6.2	.029
16.2	7730	6.1	.026
16.1	7543	6.9	.031

APPENDIX D (Continued)

Temperature (K)	Thermal Conductivity (mW/Cm·K)	Power Input (mW)	ΔT(K)
15.5	8136	6.7	.027
14.2	8867	6.1	.023
14.0	8933	6.9	.026
13.0	9054	7.1	.026
12.5	8894	7.0	.026
12.0	8906	6.9	.026
11.6	8534	6.7	.026
11.0	8789	6.1	.023
10.9	8433	7.0	.028
10.0	7777	6.4	.027
9.0	6798	5.3	.026
8.7	6594	6.1	.030
7.8	5449	5.3	.033
6.9	4453	5.1	.037
6.0	3412	5.2	.051
5.5	2979	5.2	.059
4.9	2326	4.4	.060

APPENDIX E

TABULATION OF DATA FOR SAMPLE PQ-S (IRRADIATED)

Heat Leak Apparatus (3.5 to 140K) - L/A = 33.94

Temperature (K)	Thermal Conductivity (mW/Cm·K)	Power Input (mW)	ΔT(K)
106.0	212	5.1	.820
99.4	239	6.9	.970
93.7	252	6.9	.920
84.5	293	7.0	.800
82	303	6.9	.770
78.3	334	7.0	.700
70.7	369	7.2	.660
64.0	429	7.1	.560
61.4	450	6.7	.500
58.1	528	6.7	.430
54.4	559	6.7	.410
48.6	692	5.7	.280
37.7	1122	7.7	.230
35.6	1247	7.3	.190
32.5	1514	7.5	.160
30.5	1748	7.5	.140
28.5	2045	7.4	.120
27.5	2240	7.3	.110
25.8	2575	7.2	.095
24.3	2954	8.4	.090
22.5	3664	5.6	.052
21.3	4052	6.9	.057
20.2	4520	7.1	.053
18.7	5426	6.9	.043
17.3	6197	7.0	.038
15.9	7335	7.0	.032
14.4	8296	7.4	.030
13.4	8856	7.1	.027
12.5	9157	7.2	.026
11.6	9257	7.2	.026
10.8	9374	7.2	.026
10.5	9237	6.3	.023
9.8	8317	4.3	.017
7.4	5651	7.3	.040
6.5	4714	7.3	.050
5.9	4034	7.3	.060
5.3	3415	7.3	.070
5.0	3090	4.4	.040

APPENDIX F

TABULATION OF DATA FOR SAMPLE PQ-E11 (AS-RECEIVED)

Heat Leak Apparatus (3.5 to 140K) - L/A = 24.43

Temperature (K)	Thermal Conductivity (mW/Cm·K)	Power Input (mW)	ΔT(K)	λ/T^3 (mW/Cm·K^4)
78.5	270	9.4	.850	0.0
47.8	620	12.1	.470	0.0
42.6	757	12.3	.390	0.0
35.5	1075	12.3	.270	0.0
29.5	1777	12.3	.169	0.1
26.0	2324	12.4	.130	0.1
21.2	3995	12.3	.075	0.4
17.4	7208	12.3	.040	1.4
14.8	10377	12.2	.028	3.2
12.9	12657	12.2	.023	5.9
11.5	13026	12.2	.022	8.5
10.5	13002	11.3	.021	11.2
9.5	12289	11.6	.023	14.3
8.0	10133	9.4	.022	19.8
7.5	9160	9.4	.025	21.7
7.0	8191	9.3	.027	23.8
6.5	7193	9.2	.030	26.2
5.9	6106	7.3	.029	28.8

Helium Pot Apparatus (1.5 to 4K) - L/A = 24.43

4.03	2720	9.2	.082	41.7
3.65	2133	3.0	.034	43.8
3.65	2168	5.3	.059	44.1
3.31	1525	5.1	.080	42.0
2.92	1134	2.8	.059	45.5
2.5	654	0.8	.030	41.8
2.12	417	0.6	.037	43.7
1.61	155	0.6	.102	37.1

APPENDIX G

TABULATION OF DATA FOR SAMPLE PQ-E11 (IRRADIATED)

Heat Leak Apparatus (3.5 to 140K) - L/A = 24.43

Temperature (K)	Thermal Conductivity (mW/Cm·K)	Power Input (mW)	ΔT(K)	λ/T^3 (mW/Cm·K^4)
78.8	261	12.0	1.13	0.0
44.7	685	12.3	.441	0.0
39.9	886	12.2	.338	0.0
35.0	1136	12.0	.259	0.0
30.0	1570	12.2	.190	0.1
23.9	2720	12.1	.109	0.2
19.2	4584	12.0	.064	0.6
16.9	7333	12.1	.040	1.5
14.8	10923	12.0	.027	3.3
13.5	12745	11.6	.022	5.2
12.0	12923	11.3	.021	7.5
10.8	13429	12.0	.021	10.6
10.0	12652	11.1	.021	12.6
8.5	10735	11.2	.025	17.5
7.5	8921	11.1	.030	21.1
6.5	6822	11.2	.040	24.8
6.2	5967	11.2	.045	25.0
6.0	5378	8.4	.038	24.9
5.8	5142	5.5	.020	26.3
5.7	4545	4.1	.025	24.0
5.5	4023	4.1	.029	23.5
5.2	3564	3.5	.027	24.6
5.0	3107	2.7	.024	24.8
4.7	2647	2.2	.023	24.7
4.5	2257	1.7	.021	24.7
4.3	1997	1.3	.019	25.1
4.1	1758	1.1	.017	25.5

Helium Pot Apparatus (1.5 to 4K) - L/A = 24.43

3.72	1460	7.7	.129	28.3
3.08	983	6.1	.152	33.6
2.95	940	8.4	.218	36.6
2.53	584	3.4	.142	36.0
1.96	299	.6	.050	39.7
1.64	201	.5	.059	45.5

APPENDIX H

TABULATION OF DATA FOR SAMPLE PQ-E11 (SWEPT)

Heat Leak Apparatus (3.5 to 140K) - L/A = 26.74

Temperature (K)	Thermal Conductivity (mW/Cm·K)	Power Input (mW)	ΔT(K)	λ/T^3 (mW/Cm·K^4)
13	19376	14.0	.019	8.8
10.5	23241	14.2	.016	20.0
9.0	19917	11.1	.014	27.3
7.5	13795	14.7	.028	32.7
6.5	9407	14.7	.040	34.2
6.1	8611	12.7	.039	37.9
6.0	7854	13.0	.044	36.3
5.8	7436	11.0	.039	38.1
5.6	6365	8.6	.036	36.2
5.3	5585	8.3	.039	37.5
5.0	4589	5.3	.030	36.7
4.8	3964	3.8	.024	35.8
4.5	3198	1.9	.015	35.0
4.2	2463	1.1	.012	33.2
4.0	2049	0.7	.009	32.0
3.7	1572	0.7	.011	31.0

Helium Pot Apparatus (1.5 to 4K) - L/A = 26.74

4.1	2314	10.2	.117	33.5
3.7	1877	7.5	.100	37.0
3.0	1152	8.3	.190	42.6
2.55	724	5.2	.190	43.6
2.17	502	2.6	.140	49.1
1.85	336	1.1	.080	53.0
1.7	265	.6	.050	53.9

APPENDIX I

THE FORTRAN IV PROGRAM TO SOLVE THERMAL

CONDUCTIVITY INTEGRAL, EQUATION (27)

```
FORTRAN IV      V01C-03F   MON 03-MAR-80 01:04:41                PAGE 001

0001          IMPLICIT REAL*8(A-H,O-Z)
0002          COMMON TETA,AL,U,AN1,BN1,BN2,AA,AK,HH,PI,M,I,T,A,Z1,BN3,XO1,XO2
0003          TETA=470.D0
0004          U=4.975E
0005          ACCEPT 20,AA,AN1,BN1,AL,BN2
0006       20   FORMAT(4X,F5.2,3F8.3,E12.5)
0007          TYPE 20,AA,AN1,BN1,AL,BN2
0008           ACCEPT 22,BN3
0009       22   FORMAT(5X,E12.5)
0010           TYPE 22,BN3
0011          AK=1.38E-23
0012          HH=1.0546E-34
0013          PI=3.1415926D0
0014          T=1.0D0
0015          DO 499 I=1,28
0016          T=T+.5D0
0017          Z=TETA/(AA*T)
0018          Z1=(AK*T)/HH
0019          A=1.E-5
0020          TN=TETA/T
0021          IF(TN.GT.20.D0) GO TO 1
0023          B=TN
0024          GO TO 2
0025       1    B=20.D0
0026       2    H=B-A
0027          TP=(F(A)+F(B))*H/2.D0
0028          SI=0.0D0
0029          DEF=0.0D0
0030          DO 200 MN=1,7
0031          H=H/2.D0
0032          S=0.000
0033          N=2.D0**(MN-1)
0034          DO 100 K=1,N
0035          S=S+F(A+(2*K-1)*H)
0036       100   CONTINUE
0037          TS=TP
0038          TP=TP/2.D0+S*H
0039          SIM=SI
0040          SI=(4.D0*TP-TS)/3.D0
0041          IF(N.EQ.1) GO TO 200
0043          D=DABS(SI-SIM)*1.D0/15.D0
0044          DEF=D/((2.D0*H)**4.D0)
0045          MNM=MN-1
0046       200   CONTINUE
0047          ALAMDA=(SIM*Z1*Z1*BK*Z1/(2.D0*PI*PI*U))*1000.000
0048             ALAMDA=ALAMDA*TETA*T
0049          TYPE 802,AAM,T,ALAMDA,BL,AMDA
0050       802   FORMAT(1H0,I2,4X,F5.2,3X,F7.2,3X,F5.2)
0051       499   CONTINUE
0052          STOP
0053          END
```

APPENDIX I (Continued)

```
FORTRAN IV      V01C-03F    MON 03-MAR-80 21:06:54                PAGE 001

0001          DOUBLE PRECISION FUNCTION F(X)
0002          IMPLICIT REAL*8(A-H,O-Z)
0003          COMMON TET0,AL,U,AN1,BN1,BN2,AA,AK,HH,PI,W,Z,T,A,Z1,BN3,X01,X02
0004          TC1=U/AL
0005          TC2=6N1*T**4 D0*X**4 D0
0006          B1=BN1*T**3 D0*X**4
0007          B2=BN2*T**3 D0*X**4
0008          E3=DEXP(Z)
0009          TC3=B2/E3+B1
0010           TC4=(BN3/(T**T**4-44100)**(T**T**4)/(T**T**4-44100))
0011          TC=TC1+TC2+TC3+TC4
0012          TC=1.D0/TC
0013          E1=DEXP(X)
0014          E2=E1-1.D0
0015          X2=X**4
0016          F=(E1*X2*TC/E2)*(X2.E2)
0017          RETURN
0018          END
```

VITA[2]

Mohammad-Reza Jalilian-Nosraty

Candidate for the Degree of

Doctor of Philosophy

Thesis: LOW TEMPERATURE THERMAL CONDUCTIVITY OF IRRADIATED AND SWEPT SYNTHETIC QUARTZ

Major Field: Physics

Biographical:

Personal Data: Born in Mashhad, Iran, 23 May 1946, the son of Mr. and Mrs. Jalilian-Nosraty.

Education: Graduated from Nadershah High School, Mashhad, Iran, in May, 1966; received Bachelor of Science degree in Physics from Mashhad University in May, 1972; received Master of Science degree in Physics from Oklahoma State University, in July, 1977; completed requirements for the Doctor of Philosophy degree at Oklahoma State University in May, 1980.

Professional Experience: Physics Lab Instructor at Mashhad University, Mashhad, Iran; 1973-1974; Graduate Teaching Assistant in the Physics Department at Oklahoma State University 1975-1980.